THE ASTROPHYSICAL JOURNAL SUPPLEMENT SERIES, 132:233–251, 2001 February

HYDROGENATION AND CHARGE STATES OF PAHs IN DIFFUSE CLOUDS. I. DEVELOPMENT OF A MODEL

VALÉRY LE PAGE, THEODORE P. SNOW, AND VERONICA M. BIERBAUM
Department of Chemistry and Biochemistry and Center for Astrophysics and Space Astronomy, University of Colorado, Boulder, CO 80309
Received 1999 December 20; accepted 2000 August 29

ABSTRACT

A model of the hydrogenation and charge states of polycyclic aromatic hydrocarbons (PAHs) in diffuse clouds is presented. The main physical and chemical processes included in the model are ionization and photodissociation in the interstellar UV field, electron recombination with PAH cations, and chemistry between PAH cations and major interstellar species present in the diffuse medium, such as H_2, H, O, and N atoms. A statistical model of photodissociation is presented, which is a simplified version of the Rice-Ramsperger-Kassel-Marcus theory. The predictions of this new approach have been successfully compared to experimental results for small PAH cations, justifying the application of the model to larger PAHs for which no experimental data are available. This simplified statistical theory has also been used to estimate the importance of the dissociative recombination channel in the reaction between PAH cations and electrons. Recent experimental results obtained on the chemistry between PAH cations and H_2, H, O, and N atoms are discussed and included in the model. Finally, a discussion is presented on other important processes which may affect the PAH distribution in the interstellar medium, such as electron attachment, photodetachment, photofragmentation with carbon loss, double ionization, and chemistry between PAH cations and minor species present in diffuse clouds. The results obtained with this model for compact PAHs ranging from benzene to species bearing up to 200 carbon atoms are discussed in a separate paper.

Subject headings: ISM: clouds — ISM: molecules — molecular processes

1. INTRODUCTION

The diffuse interstellar bands (DIBs) are weak absorption features seen in the spectra of reddened stars. Ranging from the near-UV to the near-IR, about 200 of these bands have been recognized with a wide diversity in width, shape and intensity (Jenniskens & Désert 1994). Many carriers have been proposed since the discovery of the features in 1921 (Heger 1922), but in the past few years most investigators have focused on carbonaceous molecules (e.g., Tielens & Snow 1995). There is still considerable debate on this issue, but the recent resolution of substructure in a few of the DIBs (Sarre et al. 1995; Jenniskens & Désert 1993), which could be interpreted as evidence for rovibrational lines of a molecular carrier, have enhanced the interest in gas-phase molecules as potential DIB carriers.

Recently Maier and coworkers, using a resonant two-color electron photodetachment technique on mass-selected anions, have found a striking match in wavelengths and relative intensities between four known DIBs and the gas phase photodetachment spectrum of C_7^- (Kirkwood et al. 1998). Although further studies are necessary to confirm C_7^- as a DIB carrier (Galazutdinov, Krelowski, & Musaev 1999; McCall, York, & Oka 2000; Motylewski et al. 2000), this is the first experimental evidence which might identify a specific molecular carrier for any of the DIBs. However, there are other molecular species which are good candidates for DIB carriers. Polycyclic aromatic hydrocarbons (PAHs, Fig. 1) have been the subject of considerable experimental work since Léger & Puget (1984) pointed out that these molecules should be ubiquitous in the interstellar medium. This suggestion was based on the good match between the unidentified infrared emission features (UIRs) seen in many environments where strong UV fields are present and the spectroscopic properties of PAHs. The proposal that PAH cations and radicals could be the carriers of the DIBs (Crawford, Tielens, & Allamandola 1985; van der Zwet & Allamandola 1985; Léger & d'Hendecourt 1985) stimulated studies of the visible absorption spectra of PAH cations in matrices. While neutral closed-shell species do not absorb in the visible region due to the relatively large energy gap between the highest occupied π level and the lowest unoccupied π^* level, PAH radical cations display a different behavior due to the incomplete filling of the last π orbital, which allows visible electronic transitions to occur within the underlying π bonding orbitals (Fig. 2). This has led to the suggestion that PAH cations (PAH^+) might be responsible for the DIBs.

Experiments have verified that PAH cations do display optical spectra in the wavelength regions where the DIBs are common. Most of these experiments were done with PAH ions in rare gas matrices (e.g., Salama & Allamandola 1992a, 1992b). The PAH cations usually display a single strong band, but none of the bands observed to date match known DIBs. Wavelength shifts due to matrix effects complicate the situation, a problem that can be overcome by gas-phase measurements (Romanini, Biennier, & Stoeckel 1999; Pino, Boudin, & Bréchignac 1999). Additional definitive measurements are expected in the near future. There are now so many known DIBs, however, that some coincidences will inevitably occur, and additional criteria will be necessary for a definite identification.

The family of PAHs and their ions is enormous, and it will be impractical to perform laboratory measurements on all of the possible species. Therefore, before selecting the most appropriate candidates for study as potential DIB carriers, it is useful to analyze the physical and chemical properties of PAH cations in order to predict which of these species are most likely to survive in the interstellar environments where the DIBs are formed. It is the purpose of this paper to develop a model for this analysis.

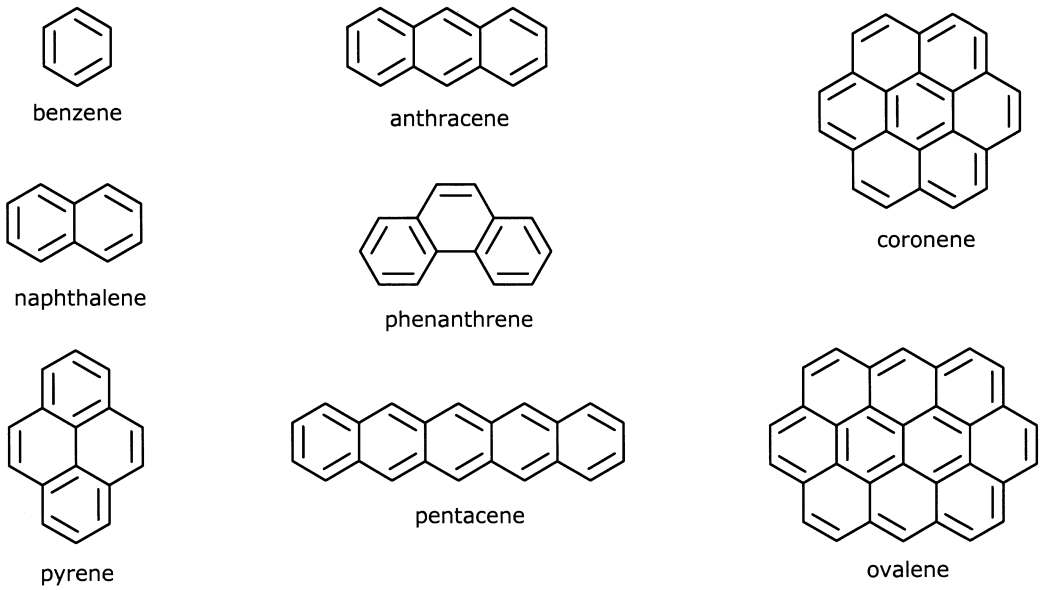

FIG. 1.—Examples of polycyclic aromatic hydrocarbons. Pyrene, coronene and ovalene are compact (pericondensed) PAHs which are thought to be more resistant to the UV field than noncompact (catacondensed) PAHs such as phenanthrene or pentacene. The peripheral hydrogen atoms have not been represented for clarity.

Without assessing the question of the formation of PAH^+ or large molecules in the interstellar medium (ISM) (Frenklach & Feigelson 1989; Cherchneff, Barker, & Tielens 1991, 1992; Allain, Sedlmayr, & Leach 1997; Bettens & Herbst 1995, 1996), and taking a very general definition of a PAH as a molecule having a well-defined carbon skeleton, there are many different classes of PAH molecules. These may differ by the state of ionization, the hydrogen coverage on peripheral carbon atoms, or the multiple isomeric forms that may exist for a given hydrogen and carbon content.

In our model we examine how a particular PAH skeleton is distributed among its various hydrogenation and charge states, depending on the physical parameters of the environment in which the PAH is immersed. For example, if we choose a PAH with a skeleton similar to pyrene ($C_{16}H_{10}$, see Fig. 1), our model investigates the relative proportion of all PAHs with such a skeleton but with different hydrogen coverage or charge states. Our model deals only with processes affecting the hydrogen coverage and charge states, without taking into account processes that may alter the carbon structure itself (e.g., photodissociation with carbon ejection or isomerization).

The formation process for large PAHs probably occurs through radical-molecule or ion-molecule reactions involving atomic carbon (C or C^+) as well as carbon-bearing molecules such as C_2H_2 (Frenklach & Feigelson 1997; Allain et al. 1997). However, in the diffuse medium, the low density of atomic carbon (neutral or ionized) with respect to H and H_2, along with the relatively high intensity of UV flux in diffuse clouds, ensures that ionization and hydrogenation will occur on shorter timescales than the conversion of one carbon frame structure to another through reactions with carbon. A typical time for C^+ insertion in a neutral PAH bearing 30 carbon atoms is 500 yr if the reaction proceeds efficiently at the Langevin collision rate. This is to be compared to the shorter times of a few years for H addition, photoionization, or electron recombination. We therefore assume that the steady state distribution of a generic PAH (i.e., with a well-determined carbon skeleton but with an unknown hydrogen coverage), over all its different charge and hydrogenation states, is reached before any competing process affecting the carbon frame can occur.

In this paper we present a model of such a system where the competition between photoionization, photodissociation, electron recombination and association reactions with hydrogen is analyzed for the purpose of predicting what kinds of PAHs are the most likely to dominate in the diffuse ISM, depending on the local physical environment.

The paper is organized as follows: after a short discussion in § 2 of typical diffuse interstellar cloud environments, § 3 describes each process that is incorporated in the model, including a discussion of the experimental work from which the various rate coefficients and cross sections are derived. A statistical Rice-Ramsperger-Kassel-Marcus (RRKM) approach is developed to estimate properties which are not currently available from experiment. Section 4 describes the model and its mathematical framework. The conclusions are summarized in the last section, and the Appendix shows how the model is applied in a simple case. The full discussion of the predictions of the model and its astrophysical implications is presented in Paper II (Le Page, Snow, & Bierbaum 2001).

2. THE DIFFUSE CLOUD ENVIRONMENT

Diffuse clouds are characterized by a low density of atomic hydrogen, ranging from about one to a few hundred particles per cubic centimeter, and a high UV radiation flux which prevents the survival of most molecules. In this section we describe our assumptions regarding both parameters.

Values for diffuse-cloud densities are commonly derived from atomic ionization equilibrium calculations (e.g., Morton 1975) or from the analysis of fine-structure excitation in atomic species (Bahcall & Woolf 1968; York & Kinahan 1974; Jenkins & Shaya 1979). From such studies a range of values between 0.1 and several hundred hydrogen

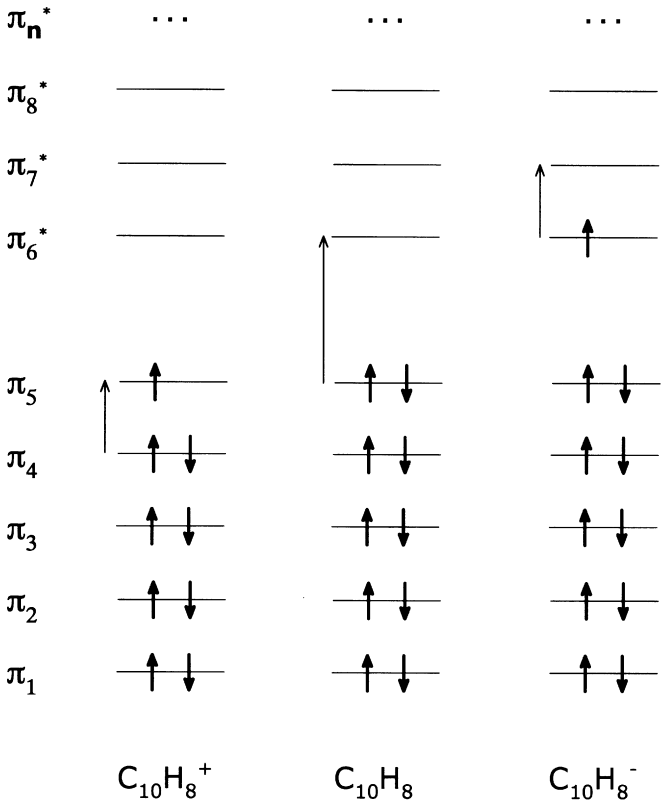

FIG. 2.—Schematic diagram of the π energy levels involved in PAH electronic transitions. The small arrows represent electrons. A cation such as $C_{10}H_8^+$ can absorb in the visible region because transitions from level 4 to level 5 are allowed and require relatively low energy. Neutrals cannot absorb in the visible because the only allowed transitions involve promotion of an electron from a π bonding level (1, 2, 3, 4, or 5) to an antibonding π^* level (6, 7, 8, ...); these higher energy transitions occur in the UV. Anions can absorb in the visible region because there is an allowed, low-energy transition from level π_6 to level π_7. For hydrogenated or dehydrogenated PAHs the situation may differ. For example, $C_{10}H_7^+$ is a singlet molecule (i.e., all electrons are paired) and its energy diagram resembles that of $C_{10}H_8$; there are no transitions in the visible. Thus, the important factor is not whether the PAH is a cation, neutral, or anion but whether or not a particular PAH is a radical. Small radicals have transitions in the visible while closed shell species generally do not. The energy gap between π levels and π^* levels decreases for large PAHs. The size for which neutral closed shell PAHs can absorb in the visible has been estimated by Salama and coworkers (Salama et al. 1996) to be about 30 carbon atoms.

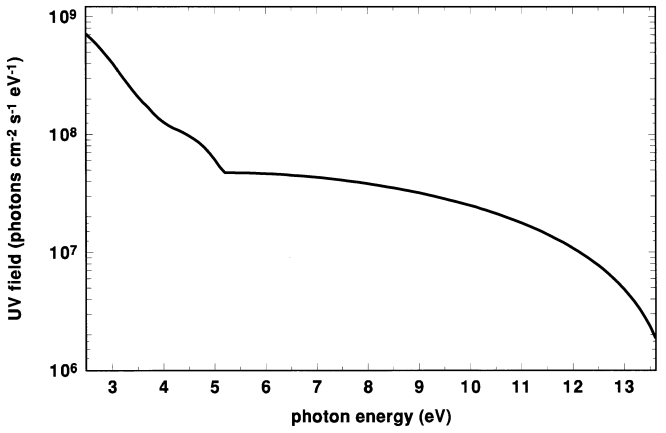

FIG. 3.—Normal interstellar UV field between 5 and 13.6 eV from Draine (1978). The range has been extended to lower energies according to the study of Mathis et al. (1983) as found in Dartois & d'Hendecourt (1997).

nuclei per cubic centimeter is determined for the kinds of clouds where the diffuse interstellar bands are formed. Thus, our PAH models are confined to this range in n_H.

The hydrogen density is kept as a variable parameter in the model (ranging from 0.1 to 1000 cm^{-3}), while the electron density is assumed to be equal to the carbon density, on the assumption that all the carbon in the diffuse ISM is singly ionized. Thus, the electron density n_e is a constant fraction of the hydrogen density n_H, and we have n_e/n_H = C/H. Recent measurements of the gas-phase C^+ abundance in diffuse clouds, using the Goddard High Resolution Spectrograph (GHRS) on the *Hubble Space Telescope*, have shown that the C/H ratio is about 1.4×10^{-4} and is roughly constant (Sofia 1997). The gas-phase ratios O/H and N/H are also constant in diffuse clouds with values of 3.2×10^{-4} and 6.0×10^{-5}, respectively (Meyer et al. 1997). Although diffuse clouds are not homogeneous, we assume a constant local density for all elements. We also assume a constant temperature of 100 K for the entire cloud.

The ultraviolet radiation field is often described using a single parameter G_0 (Habing 1968), which represents the intensity and spectral shape of the field between 6 and 13.6 eV. The omission of energies lower than 6 eV is a problem for our studies, however, because processes such as photodetachment or photodissociation can be driven by these low-energy photons. Hence, we cannot rely on this simple approximation for the radiation field. Instead we adopt the field of Draine (1978; Fig. 3), which includes the low-energy end of the energy distribution. We use the analytical expression given in Allain et al. (1996a, 1996b) to estimate the UV field between 5 and 13.6 eV, and an extension to lower energies from Mathis, Mezger, & Panagia (1983), as found in the paper of Dartois & d'Hendecourt (1997).

3. THE PHYSICAL AND CHEMICAL PROCESSES ALTERING PAHS IN THE DIFFUSE MEDIUM

In this section we discuss the main processes which alter the PAH hydrogenation and charge states in diffuse clouds. The four major competing processes are photodissociation following UV absorption, photoionization of neutral PAHs, recombination of PAH cations and electrons, and chemistry involving PAH cations and atomic and molecular hydrogen. Other minor processes are discussed at the end of this section. In the following subsections we describe each process and the sources of the rates that we adopt for the model calculations.

3.1. *Photodissociation of PAHs*

Although there are no measurements of photodissociation rates for very large PAH neutrals or cations, we can take advantage of the recent measurements carried out on smaller species (up to the coronene cation) and extrapolate these results to larger PAHs with the aid of statistical theories. After absorption of an UV photon of given energy, a PAH can either dissociate or stabilize by emitting IR radiation. The rate of this IR emission is typically about 10^2 s^{-1} and thus the dissociation will occur only if the photodissociation rate is greater than 10^2 s^{-1}. When the photodissociation rate is much lower the PAH can be considered to be photostable for that radiation.

3.1.1. *General Processes of Photodissociation*

The dissociation of PAH neutrals is expected to be different from the dissociation of cations because of the greater

number of available electronic states for the cation after dissociation. Indeed, when a neutral species like C_6H_6 loses a hydrogen atom, the remaining radical fragments, C_6H_5 and H, each have only a single electronic configuration available at low energy with the unpaired electron on the phenyl fragment occupying a nonbonding orbital (Fig. 4). For a benzene cation, the picture may be very different. Before dissociation the aromatic ring contains five electrons (rather than six for the neutral case), and thus there is an available orbital for the remaining unpaired electron after photodissociation. This configuration may have a lower energy than in the neutral case. For the benzene cation the energy is decreased about 1 eV (Klippenstein 1997), and this explains why the CH bond energy is much lower for $C_6H_6^+$ than for C_6H_6 (i.e., the dissociation $C_6H_6^+ \rightarrow C_6H_5^+ + H$ requires about 3.8 eV whereas the dissociation $C_6H_6 \rightarrow C_6H_5 + H$ requires 4.8 eV). The rearrangement of the electronic configuration in $C_6H_5^+$ involves a transition from a triplet state (two unpaired electrons, one in the aromatic ring and the other in the nonbonding orbital which remains after the CH bond is broken) to a singlet state (every electron paired, with six electrons in the aromatic ring and an empty nonbonding orbital), and it is possible only because there is a sufficiently large transition probability between the two configurations in $C_6H_5^+$ (Harvey et al. 1998).

For other PAH cations the energy of the CH bond seems to be intermediate between the benzene cation case (3.8 eV) and the neutral case ($\sim$4.8 eV), with an increasing value as the size of the PAH^+ increases. This is probably because the energy gain from the transfer of the unpaired electron onto the aromatic ring is less than in the benzene case, whose stabilization due to aromaticity is known to be high.

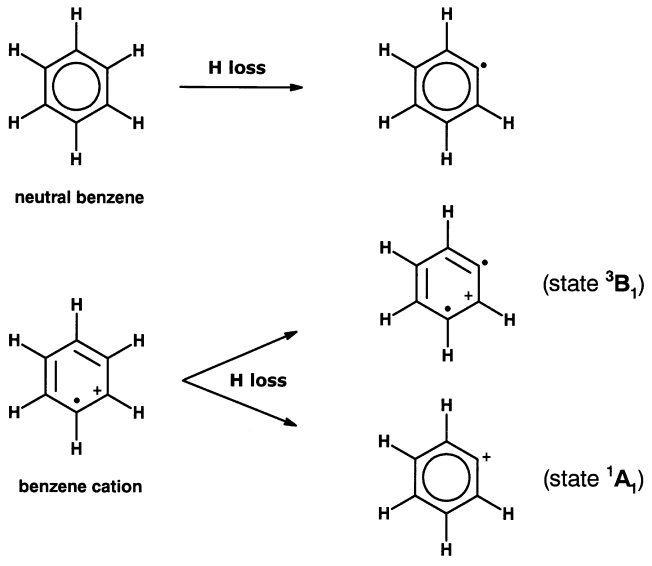

FIG. 4.—Photodissociation of benzene, showing the difference between the neutral and the cation case. Phenyl radical, which remains after H ejection from benzene, has only one electronic configuration; for neutral benzene this dissociation requires an energy of about 4.8 eV. However, for benzene cation, the species formed by H loss can access other electronic configurations in which the electron from the ruptured CH bond is captured in the π ring, thus lowering the energy of the configuration. The triplet state $^3B_1$ of the phenyl cation corresponds to an energy of 4.8 eV (Klippenstein 1997) while the singlet state $^1A_1$ has an energy 1 eV lower. The experimental CH bond dissociation energy of 3.8 eV for benzene cation is explained if a transition occurs, during photodissociation, between the triplet surface and the singlet surface.

Laboratory experiments on photodissociation have more commonly involved cations than neutrals. After the work of Neusser and coworkers in 1986 on the benzene cation (Kühlewind, Kiermeir, & Neusser 1986), new experiments have been carried out on the same system by Klippenstein, Faulk, & Dunbar (1993). Extensions to naphthalene, azulene, anthracene, phenanthrene, and pyrene cations have been made recently by Lifshitz and coworkers (Ho et al. 1995; Gotkis et al. 1993a, 1993b; Ling, Gotkis, & Lifshitz 1995; Ling, Martin, & Lifshitz 1997; Ling & Lifshitz 1998). In addition, another study involving many PAHs, ranging from benzene to coronene cations, has been carried out by Jochims et al. (1994).

Photodissociation experiments are often analyzed using statistical models such as the RRKM-quasi equilibrium theory (RRKM-QET), in which it is assumed that the excited molecule quickly relaxes to the ground electronic state via internal conversion. This process is expected to be fast for large molecules like PAHs, with the energy subsequently distributed over all of the vibrational degrees of freedom of the molecule. It is assumed that the energy flows freely through all degrees of freedom and that every microscopic state with a specific distribution of vibrational quanta has the same probability of occurrence, in agreement with the so-called microcanonical distribution (Illenberger & Momigny 1992).

The possible distributions of the energy among vibrational degrees of freedom define the phase space of microscopic states with equal energy. The molecule explores these states randomly through intramolecular vibrational redistribution (IVR). If the energy stored in one particular degree of freedom is higher than the dissociation energy of this bond (e.g., about 4.8 eV for a CH bond in a neutral PAH), then the molecule undergoes photodissociation by cleavage of this specific bond. A fundamental assumption of QET statistical theory is that there exists a particular geometry of the system known as the transition state (TS) which, if formed, leads to dissociation (see, for example, Forst 1973; Holbrook, Pilling, & Robertson 1996). If an excited molecule is distorted during the intramolecular redistribution of energy and reaches the geometry of the transition state, it is assumed that the system will never return to reactants but instead will dissociate to form products.

Thus, the rate of dissociation is determined by the probability that an excited molecule will reach the transition state during IVR. Figure 5 shows a schematic picture of the process of bond dissociation for a simple system such as

$$C_{10}H_8^+ + h\nu \rightarrow (C_{10}H_8^+)^* \rightarrow C_{10}H_7^+ + H\,, \qquad (1)$$

where $(C_{10}H_8^+)^*$ represents the photoexcited cation. Usually transition states are roughly classified as "loose" or "tight" depending on the nature of the fragmentation mechanism. For simple bond-breaking such as CH cleavage in PAHs the transition state is usually "loose" because the transition state has a geometry in which the CH bond length is sufficiently large that the H atom appears to be only loosely connected to the remaining molecule. For such transition states there are two remaining CH bending modes (in-plane and out-of-plane) having very low frequencies of about a few hundred cm^{-1}, which are known as "disappearing" bending modes (Klippenstein et al. 1993), because they disappear during the reaction process. Conversely, when the fragmentation mechanism involves multiple bond-breaking and bond-forming processes, the

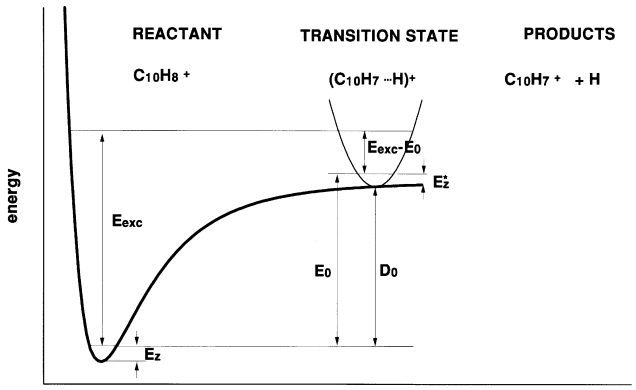

FIG. 5.—Schematic diagram of the energy needed to break a CH bond in naphthalene cation (adapted from Forst 1973, p. 56). For an excited molecule the CH distance can increase to such an extent that the molecule will reach the transition state (indicated by the parabolic curve). Breaking the bond requires that the excitation energy E_{exc} equals or exceeds E_0 (which takes into account the bond dissociation energy D_0 as well as the zero-point energies E_z and E_z^* of the reactant and transition state). If the transition state structure is reached, then $C_{10}H_8^+$ will decay to $C_{10}H_7^+ + H$. In this picture the rotational potential is assumed to be 0.

transition state has a geometry close to that of the reactant and is known as a "tight" transition state.

If the vibrational frequencies of both the reactant and the transition state are known, it is possible to evaluate the total number of microscopic states which have the same energy (E_{exc}), using mathematical methods (e.g., the steepest descent algorithm; Jeffreys & Jeffreys 1956).

In RRKM theory the rate of photodissociation after absorption of a photon of energy E_{exc} is given by the following expression:

$$k(E) = \sigma \frac{G^*(E_{exc} - E_0)}{hN(E_{exc})}, \quad (2)$$

where $N(E_{exc})$ is the density of states of the reactants at energy E_{exc}; $G^*(E_{exc} - E_0)$ is the integrated density of quantum states for the transition state; E_0 is the reaction energy threshold; h is Planck's constant; and σ is the reaction path degeneracy (i.e., the number of equivalent photodissociation processes for symmetric molecules, e.g., $\sigma = 6$ for the dissociation of benzene cation with H ejection). Thus, a RRKM calculation of a photodissociation rate coefficient requires knowledge of all frequencies of the reactant and transition state as well as the threshold energy for the specific process.

Some of the IR frequencies are known for small PAHs. See, for example, the experimental frequencies for neutrals and cations of naphthalene to coronene (Szczepanski & Vala 1993), or the theoretical IR spectrum of ionized naphthalene from ab initio quantum chemistry modeling (Pauzat et al. 1992). However, the data are scarce for larger PAHs, and sometimes theories which are simplifications of the RRKM theory are used, such as the Quantum Rice-Ramsperger-Kassel (QRRK) theory (Allamandola, Tielens, & Barker 1989) or the Rice-Ramsperger-Kassel (RRK) theory (Jochims et al. 1994). These do not require knowledge of frequencies but rather of only a few parameters which can be deduced from experiments.

At the end of this section we will propose an alternative intermediate approach which constitutes a good compromise between the semiquantitative RRK and QRRK theories and the more accurate RRKM theory, which is not easily usable because of the lack of knowledge of IR frequencies for large PAHs.

3.1.2. *Extrapolation Using the RRK Model*

Recent experiments have been found to be well represented by an RRK model calculation with two parameters. Jochims et al. (1994) have shown that in strong UV fields PAHs absorb photons which cause ionization and/or photodissociation. In these experiments the ions are created and excited with UV photons of given energy and then undergo fragmentation if the energy of the absorbed photon is sufficient. The ionic fragments are detected with a mass spectrometer coupled to a channeltron. As the time between excitation and detection is constant and estimated to be about 10^{-4} s, only PAH^+ species are probed whose energy is such that the photodissociation rate is equal to or greater than about 10^4 s^{-1}. Knowing the photon energy which leads to a photodissociation rate of 10^4 s^{-1}, an RRK extrapolation was then performed in order to estimate the energy corresponding to a photodissociation rate of 10^2 s^{-1}, which is the rate at which the radiative IR relaxation is expected to compete with dissociation.

The fragmentation process, critical for small PAHs, leads to H, H_2, and sometimes C_2H_2 losses. As the PAH becomes larger and larger, the rate of ejection of fragments decreases. It was found that PAHs of about 40 C atoms or more can absorb high-energy UV photons without undergoing fragmentation within the experimental timescale, and it was concluded that these PAHs might be photostable in the interstellar medium. This estimate was based on the extrapolation to larger PAHs of an RRK model fit to experiments on PAHs ranging from benzene to coronene. This model used the well-known expression for the dissociation rate

$$k_{diss} = \nu\left(1 - \frac{E_0}{E_{exc}}\right)^{s-1}, \quad (3)$$

where $s = 3N - 6$ is the number of degrees of freedom of the PAH, which depends on the total number of atoms N; E_{exc} is the internal energy of the molecule after excitation; E_0 is the activation energy related to bond dissociation (i.e., the minimum energy required for the fragmentation to occur), which is taken in this formula as a free parameter; and ν is the frequency factor which reflects the rate of intramolecular redistribution of the energy over all degrees of vibration of the molecule (which is related to the time required for the molecule to explore all microscopic states).

In RRK theory E_0 is assumed to be only loosely connected to the activation energy for a particular process and it was found by Jochims and coworkers that a value of 2.8 eV gave a reasonable fit for the entire set of PAHs studied for fragmentation processes leading to H and H_2 ejection. The frequency factor ν was set to 10^{16} s^{-1}, a value close to the experimental frequency factor of $10^{16.5}$ s^{-1} found by Kiefer et al. in experiments carried out on neutral benzene (Kiefer et al. 1985). Jochims et al. were able to fit their entire set of experiments with only two parameters. The existence of a good fit, while retaining all $s-1$ degrees of freedom in the model, was interpreted as evidence for an efficient intramolecular redistribution of the absorbed energy within the timescale of the experiment. It was thus concluded that there are no barriers acting to reduce the effective number of degrees of freedom available to the PAH cation for

redistributing the internal energy. Moreover, as only two parameters were needed to provide good agreement with experimental data, it was further concluded that the H atom loss mechanism was very similar for PAH^+ species of different sizes.

The fact that the RRK formula is able to closely fit the experimental values suggests that the same mechanism is working for H atom ejection in all sizes of PAH cations in the range from naphthalene to coronene. The delayed ejection of the H atom for large PAH cations is due to the increased number of degrees of freedom in which the energy can be distributed, preventing the localized storage of sufficient energy to break bonds.

3.1.3. *The RRKM Approach*

Other experiments for measuring photodissociation use the photoelectron-photoion coincidence (PEPICO) technique (Kühlewind et al. 1986, 1987), the time-resolved photodissociation (TRPD) method (Klippenstein et al. 1993), or the time-resolved photoionization mass spectrometry (TPIMS) method (Ling et al. 1995). In these experiments the rate of dissociation of the cation under investigation is monitored versus the excitation energy or versus time. Knowing the photodissociation rate at different excitation energies or times allows one to extract the threshold energy for dissociation using statistical theory. The experimental points are fitted using the more accurate RRKM curve which takes into account all frequencies of the reactants and transition state. The intercept between the fitted curve and the energy axis gives the threshold energy for the dissociation process.

The RRKM-fitted curve for the rate of photodissociation versus energy depends primarily on three parameters: E_0, N_c, and $\Delta S^{\ddagger}_{1000K}$. E_0 is the threshold energy of the dissociation process under investigation (e.g., 4.8 eV for H loss in neutral PAH) and N_c, the number of carbon atoms, is a measure of the PAH^+ size, which has a great influence on the "steepness" of the curve. For example, for a small molecule the photodissociation rate shows a steep increase with energy because there are very few vibrational degrees of freedom available to store the excess energy. Thus, the probability that a bond will break is very high for small PAH cations. Inversely, for a large molecule, there is a very low probability that sufficient energy is concentrated in one bond, due to the increasing size of the phase space. The third parameter, $\Delta S^{\ddagger}_{1000K}$, is the entropy change between reactant and transition state which determines the limit of the dissociation rate coefficient at higher energies. This parameter, which is positive for "loose" transition states and negative for "tight" transition states, can be deduced from the vibrational frequencies of reactants and transition states (as will be shown below, see eqs. [9] and [10]).

Apart from $C_6H_6^+$, which has a low threshold energy for H loss of about 3.8 eV (Klippenstein 1997; Nicolaides et al. 1997; Hrusák, Schröder, & Iwata 1997), larger PAH^+ species seem to have CH bond energies near 4.8 eV (Ling et al. 1997). Thus, if we adopt $E_0 = 4.8$ eV, the only remaining parameter is $\Delta S^{\ddagger}_{1000K}$, which depends on the structure of reactants and the transition state.

Calculating the frequencies of PAH^+ systems containing up to a few hundred degrees of freedom is computationally intensive, and we thus develop a procedure that allows us to determine the rate of dissociation versus energy for these large species without performing the full computation of the frequencies of both reactants and transition states. While the $\Delta S^{\ddagger}_{1000K}$ term strongly depends on these frequencies, this parameter does not depend on the details of these frequencies (Lifshitz 1989), but rather on the degree of tightness or looseness of the transition state. Moreover, when fitting an RRKM curve to the experimental points deduced from experiments usually the ab initio calculated frequencies are allowed to vary slightly in order to obtain the best agreement (Lifshitz 1987).

A survey of the experimental results on photodissociation of small PAH^+ species shows that the fitted curves for the photodissociation rate coefficient versus energy for the H loss channel (usually the major photodissociative channel) employ a value of about 5 cal K^{-1} for the $\Delta S^{\ddagger}_{1000K}$ term. This indicates that the H loss reaction proceeds through a "loose" transition state, as one might expect for a simple bond-breaking process. This almost constant change in entropy allows us to fully determine a photodissociation curve for large PAH cations. This RRKM fitted curve uses $E_0 = 4.8$ eV, $\Delta S^{\ddagger}_{1000K} = 5$ cal K^{-1}, and the number of degrees of freedom is deduced from the PAH size.

We can thus propose a simple procedure based on RRKM theory which allows the determination of the photodissociation rate versus energy, when E_0, $\Delta S^{\ddagger}_{1000K}$, and the PAH sizes are given. In order to do this, we have adopted a procedure inspired by the Standard Hydrocarbon Model of Dunbar, but simplified and applied to compact PAH^+ species. The standard hydrocarbon model was developed by Dunbar and coworkers (Dunbar 1990, 1997; Herbst & Dunbar 1991) in order to estimate the efficiencies of radiative association between ions and large molecules. Although the rate of radiative stabilization of a molecular complex will depend on the details of its vibrational frequencies, it was found by Dunbar that replacing the correct frequencies with rough estimates based on an "average" model hydrocarbon molecule leads to predictions which were sufficiently accurate to estimate the efficiency of the radiative association process. In this model the frequencies of the association complex [for example, as in the reaction $C_6H_5^+ + H_2 \rightarrow (C_6H_7^+)^*$] are replaced by frequencies of 3000, 1700, 1100, 700, 300, and 150 cm^{-1}, which are standard frequencies for hydrocarbons, chosen so that the total number of frequencies defining the complex is equal to the number of vibrational degrees of freedom of the molecule.

In our proposed procedure we first make the assumption that two frequencies are sufficient for a rough RRKM fit to PAH^+, namely one frequency ν_{CC} linked to the carbon skeleton and the other frequency ν_{CH} attached to the CH vibrations. We choose $\nu_{CH} = 1300$ cm^{-1} from the geometric mean of 700, 1000, and 3000 cm^{-1}, which are the "missing" vibrations when the $C_6H_6^+$ and $C_6H_5^+$ vibrations are compared at the modest ROHF/6-31g level of quantum chemistry simulation using the Gaussian 94 program package (Frisch et al. 1995). These values are also consistent with the well-known UIRs at 3.3, 8.7, and 11.2 mm, which are attributed to CH vibrations (Allamandola et al. 1989). For the carbon skeleton there are two other major UIRs, at 1600 and 1300 cm^{-1}, due to the CC aromatic stretch. In order to account for the numerous additional low-frequency vibrations around a few hundred cm^{-1}(Omont 1986), we arbitrarily choose $\nu_{CC} = 1000$ cm^{-1}.

A simple RRKM calculation with these frequencies is then carried out where rotational degrees of freedom are

neglected, but instead two CH "disappearing" bending modes are included, with frequencies of 250 cm^{-1} in order to generate a $\Delta S^{\ddagger}_{1000K}$ of about 5 cal K^{-1}. All of the frequencies are kept constant ("spectator modes") in going from reactants to transition state. One of the ν_{CH} values, corresponding to the transition state, is removed because it corresponds to the reaction coordinate.

Thus, we determine a list of frequencies for a typical PAH^+, $C_xH_y^+$. For the reactants there are $3x$–6 vibrations at 1000 cm^{-1} and $3y$ vibrations at 1300 cm^{-1}. For the transition state there are $3x$–6 vibrations at 1000 cm^{-1} and $3y$–3 vibrations at 1300 cm^{-1} together with two vibrations ν_{TS} at 250 cm^{-1}. The two low frequencies ν_{TS} correspond to the bending motion of the atom which is to be ejected, and their low value reflects the "looseness" of the transition state. Figure 6 shows the procedure in the case of the benzene cation. The rates of photodissociation versus excitation energy are computed using a modified version of the psRRKM program[1], which makes use of the steepest descent algorithm for deriving the density of states from the frequencies of both the reactant and transition states; the photodissociation rate is then calculated using equation (2).

This simplified RRKM procedure has been tested on the benzene cation. The results, presented in Figure 7, have been compared to the experiment of Klippenstein et al. (1993). There is good agreement spanning the entire energy range of their measurements: $\log_{10}(k_{Diss}(4.5\ eV)) = 3.19$ compared to 3.15 (experimental) and $\log_{10}(k_{Diss}(5.5\ eV)) = 6.1$ compared to 6.2. The procedure was then compared to the results from Lifshitz and coworkers on the naphthalene and anthracene cations. We have not made a comparison for the pyrene cation, even though data are available, because we expect this ion to exhibit peculiar behavior due to the triplet nature of $C_{16}H_9^+$ in its ground state, which is reflected by a different value for $\Delta S^{\ddagger}_{1000K}$ of about 10 cal K^{-1} (Ling et al. 1995; Le Page et al. 1999a, 1999b). Reasonable agreement was found for naphthalene: $\log_{10}(k(7\ eV)) = 3.9$ compared to 3.7 and $\log_{10}(k(10\ eV)) = 7.5$ compared to 7.3; and for anthracene: $\log_{10}(k(7.9\ eV)) = 2.2$ compared to 2.0 and $\log_{10}(k(13.6\ eV)) = 7.6$ compared to 7.5. (Two energy values were checked in each case to determine whether the general shape of the estimated RRKM curve is in good agreement with the experimental fitted curve.)

[1] Speir, P. 1993, University of Georgia, School of Chemical Sciences. Available at http://amstersgi.chem.uga.edu/software.html.

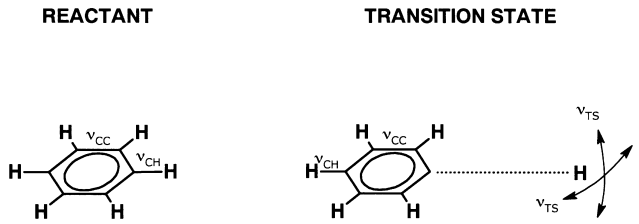

FIG. 6.—Modeling of the frequencies of the reactant and transition state for benzene molecule. The reactant is modeled as a collection of 30 harmonic oscillators, 12 of which have frequencies ν_{cc} of 1000 cm^{-1} corresponding to the carbon skeleton and the remaining 18 have frequencies ν_{CH} of 1300 cm^{-1} corresponding to the CH vibrations. If the molecule is excited with sufficient quanta in a CH bond, the system will decay with the subsequent ejection of an H atom. In the transition state configuration, one of the CH bonds is close to rupture and has been elongated; thus the two bending modes associated with the CH bond have been reduced to 250 cm^{-1} and the stretching mode has been suppressed because there is no periodic oscillation but, rather, a simple passage to the transition state followed by H ejection.

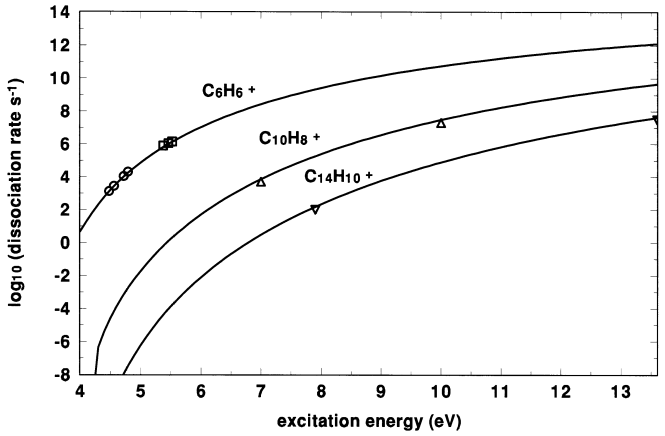

FIG. 7.—Our 2ν-RRKM fitting for the benzene, naphthalene, and anthracene cations. The circles and the squares represent experiments on the benzene cation by Klippenstein et al. (1993) and Kühlewind et al. (1986), respectively. The triangles and inverted triangles are from the experiments from Lifshitz and coworkers (Ho et al. 1995; Ling & Lifshitz 1998). The agreement is good between our fitting and the RRKM models which use the complete set of experimental or calculated frequencies.

The success of our method for $C_6H_6^+$, $C_{10}H_8^+$, and $C_{14}H_{10}^+$ (Fig. 7) justifies extending this approach to larger PAH^+ species (coronene, ovalene, etc.) using a critical energy of 4.8 eV. It may be possible to further increase the accuracy of our model by varying one of the three parameters ν_{CC}, ν_{CH}, or ν_{TS}, but as the agreement was found to be very good no refinement of the parameters was attempted.

We thus have two sets of experiments on H loss due to UV absorption, each with the statistical theory that was used to interpret them (RRK or RRKM). Table 1 presents the extrapolation to large PAH^+ species that are deduced from these two sets. The predictions of photodissociation rates for large species are very different, depending on the use of the RRK or the two-frequency RRKM frame (2ν–RRKM).

3.1.4. *Extrapolation to Large PAH Cations*

In order to determine which theory is better suited for extrapolating to larger PAH^+ species, we can use an intuitive argument: we can treat the photodissociation rate of any PAH^+ at a given energy as the product of two factors, one depending on the rate at which the excited molecule moves from one microscopic configuration to another through IVR (this is the "frequency factor" ν in RRK theory); and the other one being the probability that there are enough quanta in a CH bond to break it. This latter probability can be expressed as a simple Bernoulli process in which we calculate the probability that the energy in the CH bond equals the bond energy. Such a probability has the classic form

$$P_{break} = C_n^{n_0}\, p^{n_0}(1-p)^{n-n_0}\ , \qquad (4)$$

where p is the elementary probability of finding a quantum in one oscillator out of the total number of degrees of freedom (s) of the PAH^+; n_0 is the number of quanta needed to break the CH bond; n is the total number of available quanta which depends on the excitation energy E_{exc} and the

TABLE 1

COMPARISON OF PHOTODISSOCIATION RATES FOR H ATOM LOSS PREDICTED BY THREE MODELS AT TWO PHOTON ENERGIES

	5 eV			10 eV		
SPECIES	RRK	2ν-RRKM	Binomial Law	RRK	2ν-RRKM	Binomial Law
$C_{80}H_{25}$.....	6.8	1.5	1.6	3.2	1.3	1.5
$C_{100}H_{29}$.....	12	2.3	2.4	5.4	2.0	2.3
$C_{120}H_{31}$.....	16	2.9	3.0	7.5	2.6	2.9
$C_{150}H_{41}$.....	24	3.8	4.0	11	3.5	3.8
$C_{200}H_{51}$.....	36	4.9	5.1	17	4.5	4.9

NOTES.—Values in the table are the difference $\log_{10}(k_{\rm diss}\,[C_{50}H_{21}]) - \log_{10}(k_{\rm diss}\,[{\rm PAHH}])$ and thus are scaled to the reactivity of the $C_{50}H_{21}$ species. For example, for the $C_{120}H_{31}$ species at 5 eV photon energy, the RRK model predicts a decrease of the photodissociation rate of 16 orders of magnitude with respect to $C_{50}H_{21}$, while the 2ν-RRKM procedure and the binomial law predict a decrease of only about 3 orders of magnitude. The 2ν-RRKM procedure follows closely the intuitive binomial law for these species. In contrast, the RRK procedure rapidly diverges and is not suitable for large PAHs with $N_{\rm C} > 50$.

average energy q per quantum that we choose arbitrarily to be equal to 0.125 eV (corresponding to the frequency $\nu_{\rm CC} = 1000\ {\rm cm}^{-1}$), and finally, $C_n^{n_0}$ is the number of permutations of n_0 quanta out of n quanta. Hence, $P_{\rm break}$ has the form

$$P_{\rm break} = C_n^{n_0}\left(\frac{1}{s}\right)^{E_0/q}\left(1-\frac{1}{s}\right)^{(E_{\rm exc}-E_0)/q}. \quad (5)$$

Since we are interested only in the way this probability depends on the number of degrees of freedom $s = 3N - 6$, we can express the variation of the photodissociation rate $k_{\rm diss}$, assuming that the frequency factor ν is constant for every PAH cation, as

$$\Delta \log (k_{\rm diss}) = -\frac{E_0}{q}\,\Delta \log (s) - \frac{E_{\rm exc}-E_0}{q}\,\Delta\left(\frac{1}{s}\right). \quad (6)$$

The first right-hand factor gives the major contribution.

The prediction of this binomial law is included in Table 1, where $\Delta k_{\rm diss}$ has been calculated by comparison to the hypothetical hydrogenated PAH $C_{50}H_{21}$. From this table we conclude that the 2ν-RRKM calculations are much closer to the intuitive binomial law and thus should be preferred. The RRK theory, while closely fitting the entire set of experiments of Jochims and coworkers, seems to be inappropriate for extrapolating the results to larger PAH^+ species bearing 50 or more carbon atoms. Indeed, the RRK formula can be derived from a more general quantum formulation of Kassel (Weston 1986; Barker 1980):

$$k_{\rm diss} = \nu\,\frac{(n+1)!\quad(n-n_0+s)!}{(n-n_0+1)!\quad(n+s)!}. \quad (7)$$

The subsequent derivation of the RRK formula using the Stirling formula $\ln(n!) \sim n \times \ln(n)$ is possible if we assume that s, the total number of degrees of freedom, is much smaller than the average number of exciting quanta $n = E_{\rm exc}/q$. However, for large PAHs this formulation is no longer valid, as s increases to such an extent that it may become larger than n (for instance, for coronene $s = 3N - 6 = 102$, which is near $n_{\rm max}$ at the Lyman limit, $n_{\rm max} = 13.6/q = 108$. For very large PAHs, one should use instead another approximation of Barker's formula (assuming $s \gg n$, instead of $n \ll s$) which leads to the alternate RRK formula: $k_{\rm diss} \sim \nu(n/s)^{n_0}$. It is worth noting that for $\Delta \log (k_{\rm diss})$ such a formula will lead to the expression $-(E_0/q)\Delta \log (s)$, which is precisely the major contribution in equation (6). This formula should be preferred because it closely follows the intuitive binomial law.

Thus, the 2ν-RRKM procedure is preferred for estimating the photodissociation rate for large PAH species after absorption of a UV photon, because the RRK approach is no longer valid for large species involving a large number of degrees of freedom.

3.1.5. *Specific Photodissociation Processes*

Our 2ν-RRKM procedure has been evaluated only for the simple photodissociation process where a doublet normal PAH radical cation (i.e., with one unpaired electron) loses a hydrogen atom. In our model we will consider other similar processes involving partially dehydrogenated PAH^+ as well as neutral PAHs or even highly hydrogenated PAHs, where a few carbon atoms at the periphery of the molecule are linked to two hydrogen atoms.

It is doubtful that every process can be described by the same procedure and without changing the parameters in any way. In fact, while it is highly probable that the $\Delta S^{\ddagger}_{1000{\rm K}}$ term involved in such reactions could be somewhat different from 5 cal K^{-1}, it is, however, expected that this parameter will remain positive. This is due to the fact that the processes involved in hydrogen loss are mainly simple bond-breaking, which generally do not have an activation energy. Thus, the $\Delta S^{\ddagger}_{1000{\rm K}}$ parameter should always be positive, probably ranging between 0 and 10 cal K^{-1}.

The difference in dissociation rates for a 5 cal K^{-1} process and a 0 cal K^{-1} process should be about 1 order of magnitude at very high excitation energies and only a factor of 2 or 3 at the lower energies that are relevant to the ISM as calculated from the RRK formula given in Forst (1973):

$$\nu = \frac{ekT}{h}\exp\left(\frac{\Delta S}{R}\right), \quad (8)$$

where e is the base of the natural logarithm, k is Boltzmann's constant, T is the temperature, h is Planck's constant, R is the gas constant, and ΔS is the change in entropy. The first factor in the above formula is close to the expected typical frequency for vibrational motion (few $10^{13}\ {\rm s}^{-1}$) and is further linked to the rate of energy exchange between modes ($\sim 10^{12}\ {\rm s}^{-1}$; Léger et al. 1989). The second factor accounts for the enhancement of the rate coefficient due to an increase in entropy between the reactant and transition

state. For example, if the transition state has a few very low-frequency modes, the density of states W increases because the number of ways the excitation energy can be spread over the different vibrational modes is enhanced, leading to a subsequent increase in entropy in agreement with Boltzmann's formula $S = k \ln(W)$. This explains why the overall frequency factor is sometimes much greater than the typical value of $\sim 10^{13}$ s^{-1}.

Thus, in simple bond-breaking processes, the positive change in entropy arises from the increased density of states, which is a consequence of the existence of low vibrational frequencies for the relative motion of the two fragments when the system is distorted to the geometry of the transition state.

We distinguish six different processes, three for neutrals and three for cations, leading to H atom loss after UV absorption in our model, depending on the ionization state of the PAH as well as its hydrogenation state. The three basic processes are (1) loss of an H atom from a carbon with sp^2 hybridization (i.e., bearing a single H atom); (2) loss of an H atom from a carbon with sp^3 hybridization (i.e., bearing two H atoms); and (3) H_2 loss from an sp^3 carbon. To fully determine the RRKM curves which provide an estimate of the rate coefficient for these six channels, we must assign an enthalpy of reaction to each of them plus an energy of activation where necessary. This can be done in our 2v-RRKM procedure by specifying E_0 and $\Delta S^{\ddagger}_{1000K}$ for each of the six processes. Tables 2 and 3 give the estimated energies assigned to these channels, based on known values for small PAH^+ which are found in the literature (Lias et al. 1988).

The process requiring the lowest activation energy is the ejection of a hydrogen atom from a hydrogenated PAH. This process requires an energy only slightly higher than 1 eV in the benzene case (Mebel et al. 1997), for example, and thus might be very efficient in an interstellar asymmetric UV field like the Draine field where there is a high density of low-energy UV photons. This process deserves special attention because it may be the major one preventing full hydrogenation of PAH^+. The comparison between the dissociation rate attached to this channel, which depends on the PAH size, and the rate of hydrogenation of PAHs gives directly the limiting PAH size where a normal PAH becomes fully hydrogenated, converting all the peripheral sp^2 hybridized carbon atoms into sp^3 carbon atoms, as in the multistep hydrogenation reaction $C_6H_6^+ + 6H \rightarrow C_6H_{12}^+$. Forst (1973) reported that such a process should have a $\Delta S^{\ddagger}_{1000K}$ of about 0 cal K^{-1}, following experiments performed with the C_2H_5 radical. Forst refers to these processes as Type II reactions, which are similar to Type I reactions (simple bond-breaking processes), except that there is an activation energy for the reverse process as in the reaction $C_6H_5 + H_2 \rightarrow C_6H_7$.

There is a recent ab initio study by Mebel and coworkers on the C_6H_7 system, where the authors have investigated the H/H_2 loss channel. The reactants, products and transition states were fully characterized, together with the frequencies of all species calculated using quantal modeling.

TABLE 2

EXPERIMENTAL C-H BINDING ENERGY AND ACTIVATION ENTROPY FOR SMALL PAH CATIONS

Reaction	Activation Energy E_0 (eV)	Activation Entropy $\Delta S^{\ddagger}_{1000K}$ (cal K^{-1})
Benzene:[a] $C_6H_6^+ + h\nu \rightarrow C_6H_5^+ + H$	3.8	5.7
Naphthalene:[b] $C_{10}H_8^+ + h\nu \rightarrow C_{10}H_7^+ + H$	4.5	5.6
Anthracene:[c] $C_{14}H_{10}^+ + h\nu \rightarrow C_{14}H_9^+ + H$.....	4.4	5.9
Phenanthrene:[c] $C_{14}H_{10}^+ + h\nu \rightarrow C_{14}H_9^+ + H$.....	3.9	4.4
Pyrene:[d] $C_{16}H_{10}^+ + h\nu \rightarrow C_{16}H_9^+ + H$.....	4.6	11
Larger PAH:[e] $PAH^+ + h\nu \rightarrow PAH^+_{-1} + H$.....	4.8	5.0

[a] Klippenstein et al. 1993.
[b] Ho et al. 1995.
[c] Ling & Lifshitz 1998.
[d] Ling et al. 1995.
[e] Estimation, see text.

TABLE 3

PARAMETERS EMPLOYED IN OUR MODEL FOR THE COMPUTATION OF PHOTODISSOCIATION RATES[a]

Reaction	Activation Energy E_0 (eV)	Activation Entropy $\Delta S^{\ddagger}_{1000K}$ (cal K^{-1})
$PAH^+ + h\nu \rightarrow PAH^+_{-1} + H$	4.8[b]	5.0
$PAHH^+ + h\nu \rightarrow PAH^+ + H$	2.9[c]	5.0
$PAHH^+ + h\nu \rightarrow PAH^+_{-1} + H_2$.....	3.2[c]	5.0
$PAH + h\nu \rightarrow PAH_{-1} + H$	4.8[b]	5.0
$PAHH + h\nu \rightarrow PAH + H$.....	1.2[b]	0.0[d]
$PAHH + h\nu \rightarrow PAH_{-1} + H_2$.....	1.6[b]	5.0

[a] $PAH^{(+)}$ represents a PAH (cation or neutral) with a number of H atoms equal or less than the normal number (e.g., $C_{24}H_n$ with n between 1 and 12 for the coronene molecule $C_{24}H_{12}$). $PAHH^{(+)}$ represents a highly hydrogenated PAH (e.g., with $n > 12$ for coronene).
[b] Ling et al. 1995.
[c] Deduced from the heat of formation of $C_{10}H_9^+$, $C_{10}H_8^+$, and $C_{10}H_7^+$.
[d] Deduced from the calculation of Mebel et al. 1997 on the C_6H_n ($n = 5, 6, 7$) system.

From these frequencies it is possible to estimate the $\Delta S^{\ddagger}_{1000K}$ of the reaction using the classical formula of statistical mechanics (see, e.g., Rühl, Price, & Leach 1989)

$$\Delta S^{\ddagger} = R \ln\left(\frac{Q^{\ddagger}}{Q}\right) + \frac{U^{\ddagger} - U}{T}, \quad (9)$$

where R is the gas constant, $Q^{\ddagger}$ and Q are the partition functions of transition state and reactants, respectively, U is the internal energy, and T is the absolute temperature. Taking into account only the vibrational partition functions leads to the following expression for the entropy:

$$S = R \sum_i \ln\left(\frac{1}{1 - e^{-h\nu_i/kT}}\right) + \left(\frac{h\nu_i/kT}{e^{h\nu_i/kT} - 1}\right), \quad (10)$$

where k is Boltzmann's constant, h is Planck's constant, and ν_i are the frequencies of the reactants or transition state, with the sum over all frequencies.

From this formula and the table of computed frequencies from the paper of Mebel et al. a $\Delta S^{\ddagger}_{1000K}$ of 0.06 cal K^{-1} has been calculated, in very good agreement with the low expected value for a Type II reaction. This leads to a decrease of the dissociation rate for this process with respect to a process with a 5 cal K^{-1} activation energy of about $\exp(\Delta S/R) = \exp(5/2)$ (eq. [8]), which is about 1 order of magnitude at very high energies but only a factor of a few for a 10 eV exciting photon in the RRKM frame. For this process we thus choose to compute the 2ν-RRKM curve using the more appropriate value of 0 cal K^{-1} for the H loss; this is obtained, reversing equation (10), by replacing the two low frequencies at 250 cm^{-1} with two frequencies at 950 cm^{-1}. For the other five channels a value of 5 cal K^{-1} is used for $\Delta S^{\ddagger}_{1000K}$.

For all six processes and with the values of E_0 and $\Delta S^{\ddagger}_{1000K}$ reported in Table 2 we can estimate the curve of photodissociation rate versus energy for any PAH in any hydrogenation and charge state. Figures 8 and 9 present the estimates of these two-frequency RRKM calculations for the benzene and coronene systems.

The overall photodissociation rate k_{ph} of a PAH in the ISM will depend on the cross section for UV photon absorption $\sigma_{UV}(E)$, the density of photons $N(E)$ at a particular photon energy E, and the branching ratio $k_{diss}/(k_{diss} + k'_{rad})$ which represents the competition between the radiative stabilization (rate k'_{rad}) and the photodissociative

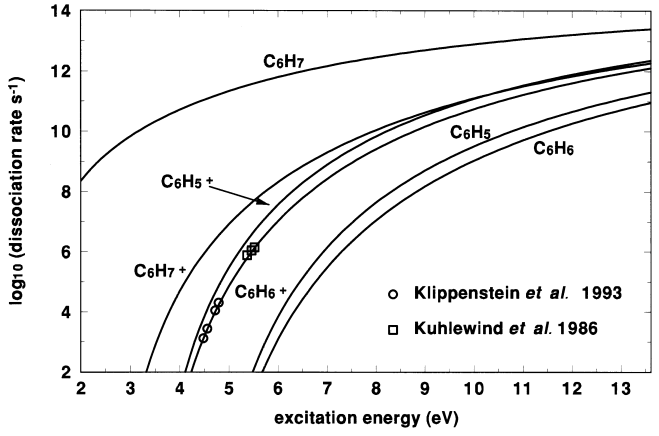

FIG. 8.—2ν-RRKM predictions for the benzene system

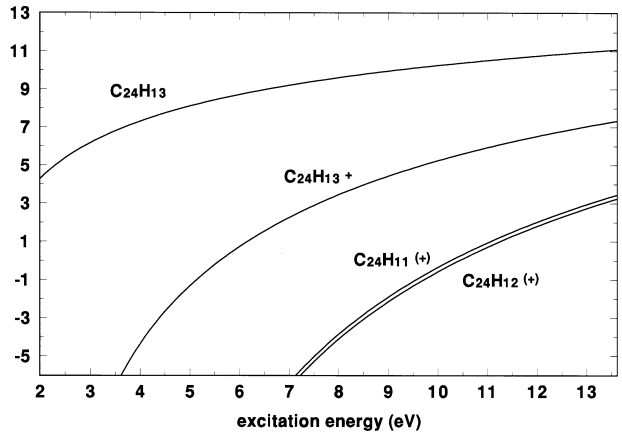

FIG. 9.—2ν-RRKM predictions for the coronene system. PAH$^{(+)}$ represents both $C_{24}H^{+}_{12}$ and $C_{24}H_{12}$.

channel (rate k_{diss}):

$$k_{ph} = \int_{IP}^{13.6} \left(\frac{k_{diss}}{k_{diss} + k'_{rad}}\right) \sigma_{UV}(E) N(E) dE . \quad (11)$$

For k'_{rad} we use the stepladder model (Holbrook et al. 1996) which takes into account the likely possibility that the emission of more than one IR photon is required in order to stabilize the molecules. Each IR photon was chosen to bear an energy q_{IR} of 0.18 eV and thus the number of photons required to stabilize the PAH is equal to $(E_{exc} - E_0)/0.18$. k'_{rad} is calculated using the following formula (Herbst & Le Page 1999):

$$k'_{rad} = k_{rad} \times \prod_{i=1}^{n} \frac{k_{rad}}{k_{diss} + k_{rad}}, \quad (12)$$

where $n = (E_{exc} - E_0)/q_{IR}$ is the number of intermediate energized complexes which must be stabilized in order to leave the PAH with an energy less than the critical energy E_0. We choose for k_{rad} the approximation given by Herbst & Dunbar (1991):

$$k_{rad} = 73 \frac{(E_{vib})^{1.5}}{s^{0.5}}, \quad (13)$$

where E_{vib} is the vibrational energy of the complex and s the total number of degrees of freedom. However, replacing the above expression by a standard energy-independent value of $k_{rad} = 10^2$ s^{-1} was found to give almost the same results for the overall rate k_{ph}. Moreover, as the calculated photodissociation rates are usually rapidly varying at least in the vicinity of the 10^2 s^{-1} range (see for instance Figs. 7, 8, and 9) the replacement of k'_{rad} in equation (11) by k_{rad} directly was found to be an acceptable approximation. Indeed, the stepladder model is more precise only in the energy range where k_{rad} and k_{diss} are competing; since this range is narrow, the stepladder model, while effectively used in this modeling, may not be required because the enhanced precision obtained in the calculation of the overall photodissociation rate is small (a few percent at best). Figure 10 is a plot of the photodissociation rates with H loss.

3.2. *Photoionization of Neutral PAHs*

Ionization of PAH neutrals in the ISM will depend primarily on the UV absorption cross section σ_{UV} and on the ionization yield $Y_{ion} = \sigma_{ion}/\sigma_{UV}$. The ionization yields for

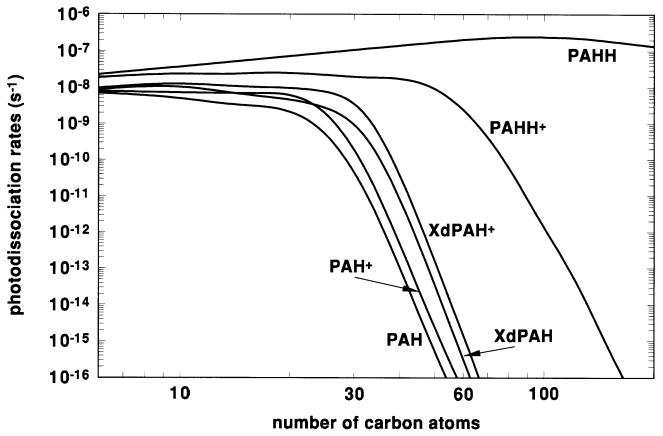

FIG. 10.—Photodissociation rate with H loss for three different classes of PAHs as a function of PAH size. XdPAH represents an extremely dehydrogenated PAH (e.g., $C_{16}H$ or $C_{24}H$), while PAHH represents a PAH bearing an extra hydrogen (e.g., $C_{16}H_{11}$ or $C_{24}H_{13}$). The rates have been calculated using the 2ν-RRKM procedure assuming a $\Delta S^{\ddagger}_{1000K}$ of 5.0 cal K^{-1} except for the reaction PAHH + $h\nu \rightarrow$ PAH + H, where a $\Delta S^{\ddagger}_{1000K}$ of 0.0 is assumed. PAH$^+$ or XdPAH$^+$ appear to be more dissociative than their neutral counterparts primarily because of the existing competitive photoionization channel in the neutral case.

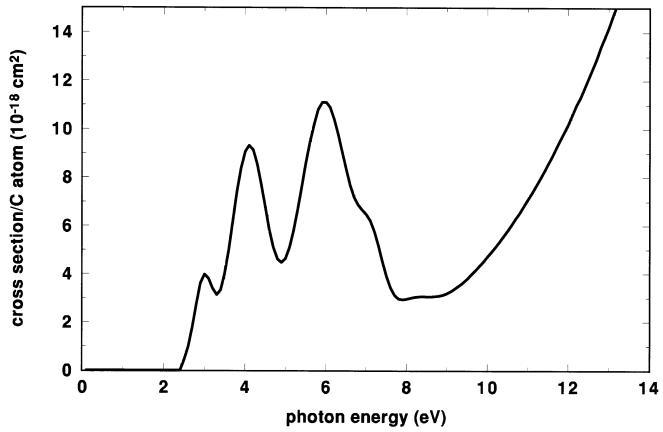

FIG. 11.—UV absorption cross section measured by Joblin (1992) for a PAH mixture with an average mass of 365 amu. The experimental curve of Joblin has been fitted using a collection of Gaussian curves.

pyrene and coronene have been measured by Verstraete et al. (1990), who found that the ionization cross sections are remarkably similar when scaled to the number of carbon atoms in the molecule. This photoionization yield shows a steep increase just above the ionization energy of the PAH molecule and reaches a value of about 0.75 at the Lyman limit (13.6 eV). We found that the ionization yield as measured by Verstraete et al. can be represented using a simple expression:

$$Y_{\rm ion} = a \times e^{-b[c(E_{\rm exc}-d)]^4}\,, \qquad (14)$$

where $a = 0.8$ is a constant giving the yield at the Lyman limit; b is a constant equal to 0.00128; $c = (12 - {\rm IP}_{\rm coronene})/(12 - {\rm IP}_{\rm PAH})$ is a parameter depending on the PAH ionization energy ${\rm IP}_{\rm PAH}$ and the ionization energy of coronene, both expressed in conventional μm^{-1} units of energy (10.96 μm^{-1} = 13.6 eV); c is the approximate energy (12 μm^{-1}) where the maximum yield is reached; and $E_{\rm exc}$ the photon excitation energy in μm^{-1}.

The UV absorption cross sections of pure PAHs have been thoroughly investigated by Joblin (1992). The UV absorption spectra of PAHs share many common features: absorption bands between 3 and 6 μm^{-1} which correspond to $\pi \rightarrow \pi^*$ transitions, and a rising continuum from around 6 μm^{-1} to the Lyman limit which corresponds to the stronger σ–σ^* transitions, with a possible contribution of $\pi \rightarrow \sigma^*$, and possibly Rydberg transitions, around 6 to 10 μm^{-1}. Soot extracts were also investigated by Joblin as they may be better analogs of interstellar PAHs. It was found that soot extracts yield results similar to those for pure PAHs. Although all PAHs under investigation display generally similar absorption curves, we choose to model the PAH UV absorption cross section using the soot extract with the largest PAHs studied by Joblin, which have an average mass of 365 amu. The corresponding experimental curve of Joblin has been fitted using a set of five different Gaussian functions centered on 2.4, 3.3, 4.8, 5.75, and 6.5 μm^{-1} and a large peak centered at 17 μm^{-1} to account for the $(\sigma + \pi) \rightarrow \sigma^*$ transitions. The fit is displayed in Figure 11.

In our model the ionization rate is estimated using the formula (Allain et al. 1996a)

$$k_{\rm ion} = \int_{\rm IP}^{13.6} Y_{\rm ion}(E)\sigma_{\rm UV}(E)N(E)dE\,, \qquad (15)$$

where $Y_{\rm ion}$ is the ion yield from the experiment of Verstraete et al. (1991), $\sigma_{\rm UV}$ is the UV absorption cross section as deduced from the work of Joblin (1992). Thus, either an absorbed photon will ionize the neutral molecule (eq. [15]) or participate in the photodissociation (eq. [11]). The results are presented in Figure 12.

3.3. *Electron Recombination*

As discussed by Duley & Williams (1984, p. 54), recombination is an important process in interstellar chemistry, since it plays a role in controlling the level of ionization and hence the rate of chemical reactions in interstellar clouds. When an electron encounters an ion AB^+, the overall recombination process is often separated into two parts: the

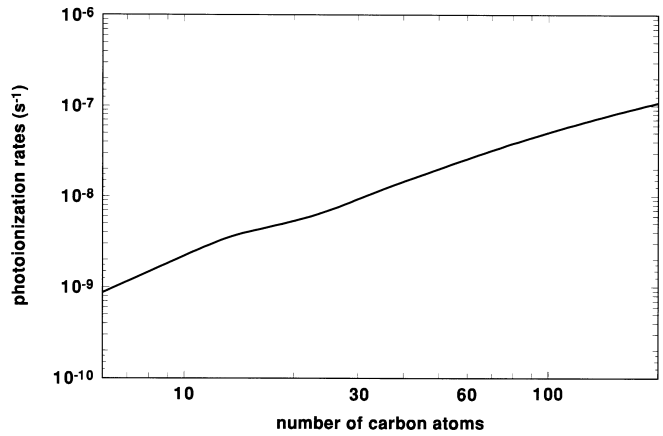

FIG. 12.—Photoionization rates of neutral PAHs calculated using eq. (15). The rate is approximately proportional to the size of the PAH; however, the decrease of the PAH ionization potential with increasing size tends to increase the fraction of absorbed UV photons that are able to ionize the molecule.

capture $AB^+ + e \rightarrow AB^*$, where AB* is an electronically excited neutral molecule, and dissociation, $AB^* \rightarrow A + B$. A simplified version of the theory shows that the dissociation rate should be proportional to $T^{-1/2}$ if a Maxwellian distribution is assumed for the electrons.

The recombination rates of PAH cations have been measured for only two species, benzene and naphthalene, with values of 10^{-6} and 3×10^{-7} cm^3 s^{-1} at 300 K, respectively (Abouelaziz et al. 1993). These values are well within the expected range for polyatomics (Bates 1988), as seen from the expression

$$k_{\rm rec} = 10^{-6}\left(\frac{100}{T}\right)^{1/2} \text{cm}^3 \text{ s}^{-1} . \quad (16)$$

Following Salama et al. (1996), we use the values from Abouelaziz for the electron capture rates in our model. An alternate approach to estimate the recombination rate between PAH cations and electrons is to consider PAHs as small grains as in the work of Bakes & Tielens (1994) and to calculate the rate using a theory of charge of grains (Draine & Sutin 1987). However, as we are concerned mainly by small PAHs with about less than one hundred carbon atoms, we chose to use the experimental measured rates of Abouelaziz et al.

A major issue in the recombination sequence between PAH cations and electrons is the degree of dissociation. Recently the question has been raised (Rowe & Rebrion-Rowe 1995) whether there is any dissociation in the recombination of large PAH^+. Unfortunately, nothing is known about the nature of the recombination products and even for small ions the data are very scarce (Adams 1994). Dissociative recombination requires a crossing between an attractive and a repulsive potential energy surface. Such crossings occur within a very short time (about a vibrational period, $\sim 10^{-13}$ s) and thus when such an event occurs, the probability for dissociative recombination is high.

A likely dissociative channel for $PAH^+ + e$ is the loss of one hydrogen atom, in parallel with the photodissociation process, because the ejection of an H atom requires the breaking of only one bond, unlike the more complex H_2 and C_2H_2 losses. When recombination occurs, we may regard the resulting neutral excited PAH as analogous to a PAH that has absorbed a UV photon: this species has additional energy equal to the recombination energy (or the ionization potential of the neutral) which is then distributed over the internal degrees of freedom of the PAH. If we assume this picture to be valid, it is possible to use the same statistical theory to calculate the branching ratio as that already employed in the photodissociation case.

The use of RRKM theory requires the assumption that after neutralization the molecule can be regarded as being in its ground electronic state with all the excitation energy distributed among the various vibrational degrees of freedom. This assumption is justified only if internal conversion occurs on a timescale shorter than the typical time needed for dissociation. Such a mechanism can occur when two different electronic states have similar energies (e.g., an excited electronic state with low vibrational energy and the ground electronic state with high vibrational energy).

In order to test this assumption, we compare this situation to that described by Buch (1989), in which it was assumed that direct H loss can occur after UV absorption, provided that the incoming photon excites one electron from a bonding σ orbital to an antibonding σ^* orbital. After this transition the molecule is in a dissociative state which rapidly produces an H atom and the remaining dehydrogenated PAH, provided that internal conversion does not induce a $\sigma^* \rightarrow \sigma$ radiationless transition. This mechanism, known as direct photodissociation, competes with internal conversion and was also postulated by Omont (1986). A tentative maximum dissociation rate for large neutral PAHs of 10^{11} s^{-1} in the ISM has been proposed for this process.

However, no evidence for this mechanism has been detected experimentally (Jochims et al. 1994). The fact that the observed behavior in laboratory measurements can be described solely with RRKM theory argues that direct dissociation is not important. This suggests in turn that internal conversion, which is the cornerstone of statistical theory, is rapid enough to prevent dissociation, thus justifying our assumption that this is also true during electron recombination. This is not unexpected because the number of available vibrational states for internal conversion increases dramatically when $E_{\rm exc}$ is comparable to the PAH ionization energy; the density of states varies roughly as $(E_{\rm exc}/q)^s$ when s is relatively small (Omont 1986) and $(s)^{(E_{\rm exc}/q)}$ when the PAH is very large. Thus, it is likely that many levels belonging to different electronic states will have almost the same energy, allowing rapid internal conversion. We conclude that the use of RRKM theory in our treatment of recombination is justified.

Accordingly, no direct dissociation process is assumed in the case of recombination between PAH^+ and electrons, and the branching ratios for dissociation with H or H_2 loss are estimated using the simplified 2ν-RRKM theory outlined in the section above. Results are presented in Figure 13 for recombination of PAH cations in their normal hydrogenation state. We can note that this figure compares qualitatively well with Figure 3 on the recombination of carbons chains in the paper of Bettens & Herbst (1995).

3.4. *Chemistry Involving PAH Cations and Atomic and Molecular Hydrogen*

Ion-neutral rate coefficients are usually much larger than the corresponding neutral-neutral rates and we thus consider only the chemistry of PAH cations. The reactivity of

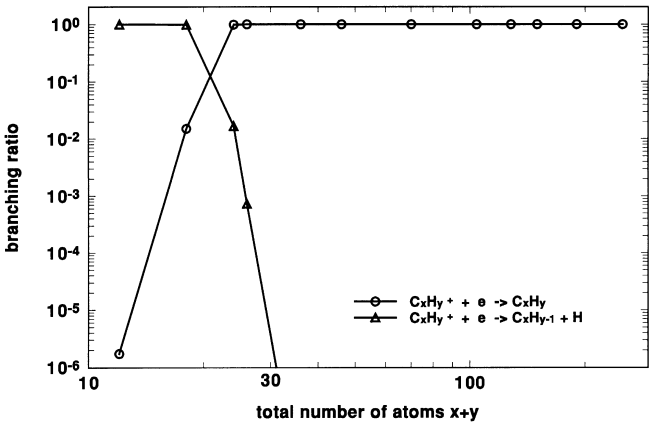

FIG. 13.—Estimation of the branching ratio of PAH^+ recombination with electrons. According to the model, the recombination is expected to be nondissociative for pyrene cation or larger PAH^+.

PAH cations seems to be independent of their hydrogenation state (radicals react with atoms while dehydrogenated closed shells react with H_2) while for neutrals only radical PAHs are reactive at the low temperatures prevailing in the ISM (reaction between closed-shell PAH and H atoms are slow because there is an activation energy, as in the $C_6H_6 + H$ reaction). Reactions between PAH radicals and H_2 are also slow (e.g., $C_6H_5 + H_2$) and thus the overall contribution of the chemistry of neutrals is expected to be small. In Paper II we justify the neglect of the neutral-neutral chemistry by presenting results of a model calculation where a rate of 10^{-10} cm^3 s^{-1} between neutral radicals and H atoms is assumed. Thus, in our model the major processes are reactions between PAH^+ and atomic and molecular hydrogen. Other reactions involving O and N atoms will be discussed later. There are a few measurements of reactivity of the smaller PAH cations such as benzene (Ausloos et al. 1989; Giles, Adams, & Smith 1989; Petrie, Javahery, & Bohme 1992; Scott et al. 1997; Capron et al. 1994), naphthalene (Le Page et al. 1997, 1999b; Feng & Lifshitz 1996), and pyrene (Le Page et al. 1999a). In these experiments the major process is H addition, here shown for the naphthalene cation:

$$C_{10}H_8^+ + H \rightarrow C_{10}H_9^+ . \quad (17)$$

Another important process is H_2 addition to the dehydrogenated cation to form protonated PAHs. Both reactions have been studied at pressures of about 1 torr ($\sim 10^{16}$ cm^{-3}) and thus it is important to extract the corresponding radiative association rate, which is relevant to the ISM. In the experiments carried out at high pressure, the complex formed between the cation and the neutral stores a quantity of energy which is equivalent to the exothermicity of the overall reaction. This energized complex can either decay back to reactants,

$$(C_{10}H_9^+)^* \rightarrow C_{10}H_8^+ + H , \quad (18)$$

or undergo collisions with the buffer gas M which removes the excess energy and thus stabilizes the complex,

$$(C_{10}H_9^+)^* + M \rightarrow C_{10}H_9^+ + M . \quad (19)$$

The typical time between successive collisions is about 10^{-7} s at 1 torr. If the excited complex has a lifetime much longer than this, the association product is likely to be generated every time a complex is formed. In the ISM the diffuse cloud density is much lower (~ 10 cm^{-3}) and this stabilizing process cannot operate because the collision time is much longer (a few years).

Hence, the only mechanism for an excited complex to be stabilized in the ISM and form the association product is emission of an IR photon before the energized complex redissociates to reactants. The emission of an IR photon occurs typically in about 10^{-2} s and thus a large termolecular association rate at high pressure does not guarantee an efficient corresponding radiative association at very low pressure unless the complex lifetime (which primarily depends on the PAH size) is greater than this typical time for IR emission.

The only experiments where the truly radiative association reaction between a PAH^+ and H_2 has been measured are for $C_6H_5^+ + H_2 \rightarrow C_6H_7^+$ (Ausloos et al. 1989) and $C_{10}H_7^+ + H_2 \rightarrow C_{10}H_9^+$ reactions (Le Page et al. 1997, 1999b), which have been measured in an ICR trap. These radiative association processes for small PAH^+ species with a relatively small number of degrees of freedom appear to be efficient, the first being equal to 1.5×10^{-11} cm^3 s^{-1} and the second to 2.2×10^{-11} cm^3 s^{-1}. The $C_{10}H_7^+ + H_2$ reaction is interesting because the energized $C_{10}H_9^{+*}$ complex is the same as that arising during the $C_{10}H_8^+ + H$ reaction, and furthermore the exothermicities of the reactions are almost identical. Since the radiative association reaction $C_{10}H_7^+ + H_2$ is efficient, one would expect the same for the radiative $C_{10}H_8^+ + H$ reaction because the complex lifetime, which drives the efficiency of the radiative association, depends principally on the total number of degrees of freedom and the exothermicity of the reaction.

Recent computer simulations using phase space theory (Herbst & Le Page 1999) have shown that while the H addition reaction to the benzene cation is not efficient due to the competing bimolecular abstraction channel $C_6H_6^+ + H \rightarrow C_6H_5^+ + H_2$, this competing channel is a minor process in the naphthalene case and the addition reaction is almost as efficient as the corresponding termolecular association. It is expected that larger PAH^+ species associate even more readily to H atoms in view of their increasing number of degrees of freedom. Therefore, in our model the association reaction rates have been chosen to equal the termolecular reaction rates. Figure 14 shows that PAH cations display a somewhat predictable chemistry with the major interstellar species H_2, H, O, and N. It is thus relatively easy to extrapolate these results to larger PAH^+. Moreover, because of the rather small temperature dependence found by Giles and coworkers (Giles et al. 1989) for the $C_6H_5^+ + H_2$ reaction and by Herbst & Le Page (1999) in the computed simulation of the $C_6H_6^+ + H$ reaction, no temperature dependence for reactions involving PAH^+ and hydrogen has been assumed.

The reactions between PAH^+ and H atoms can be understood in the following way. First we note that the SOMO (the singly occupied molecular orbital, which is also the highest occupied molecular orbital) of a PAH cation is spread over the carbon skeleton, due to the delocalization of radical character (Nourse, Cox, & Cooks 1992). When a hydrogen atom approaches a conventional PAH^+ doublet such as benzene, naphthalene or pyrene cation, it will interact primarily with this SOMO, which bears only one unpaired electron (Fleming 1976). It is tempting to suppose that the reaction will proceed only if the H atom strikes a

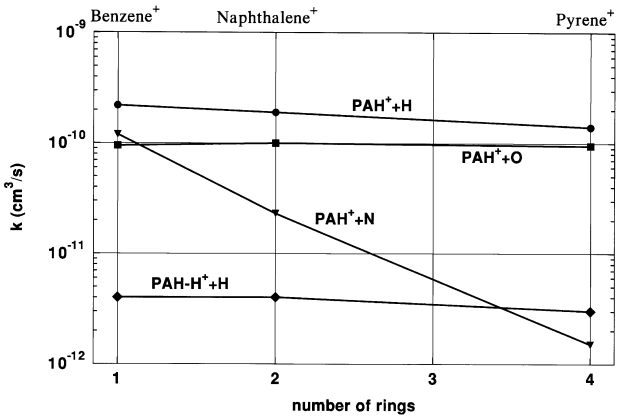

FIG. 14.—Chemistry between small PAH cations and atomic species which are relevant to the ISM.

carbon atom which is able to attach an additional H; i.e., a carbon atom that is able to convert from sp^2 to sp^3 hybridization.

Thus, a distinction can be made between the carbon atoms which are "locked" in sp^2 configuration due to structural constraints, and others which can add an H atom and simply change from sp^2 to sp^3. In this picture the rate coefficient is proportional to k_{benzene} multiplied by the ratio of "reactive" carbon atoms to the total number of carbon atoms. The "reactive" carbon atoms are the peripheral ones which already bear H atoms, because the C skeleton is not strained if these carbon atoms move from sp^2 to sp^3 hybridization.

We further assume that the rate coefficient of the reaction between the benzene cation and H atom already includes the effects of collision geometry (e.g., the probability that the H atom will not react whenever a hydrogen, rather than carbon atom, is approached). Therefore, the value of this rate coefficient (2.2×10^{-10} cm^3 s^{-1}) represents the reactivity due to attack on the carbon structure. Then the rate coefficient for $C_{10}H_8^+ + H$ should be $8/10\ k_{\text{benzene}} = 1.8 \times 10^{-10}$ cm^3 s^{-1} (experimental value: 1.9×10^{-10} cm^3 s^{-1}; Snow et al. 1998). For the pyrene cation this rate coefficient will be $10/16\ k_{\text{benzene}} = 1.4 \times 10^{-10}$ cm^3 s^{-1} (experimental value: 1.4×10^{-10} cm^3 s^{-1}; Le Page et al. 1999a).

These predictions are in very good agreement with the experimental data and do not depend on the accuracy of the rate coefficient for the benzene cation and H, but rather on the *difference* in reactivities between the benzene cation and any PAH^+. Thus, assuming a homogeneous spread of the SOMO over the reactive part of the carbon skeleton, this simple scaling method can be used to roughly estimate the rate for any $PAH^+ + H$ reaction. For example, k_{coronene} will be about 1.1×10^{-10} cm^3 s^{-1}. In the model we assume a rate coefficient at 300 K of $(y/x)\ k_{\text{benzene}}$ for any generic PAH^+, $C_xH_y^+$.

This somewhat simplistic approach can explain why, in the reaction between PAH^+ and O atoms, the rate coefficient is almost constant and equal to about 10^{-10} cm^3 s^{-1}. In this reaction any pair of adjacent carbon atoms can accept an oxygen atom without changing the geometry of the carbon structure. The formation of an epoxy structure (Le Page et al. 1999a, 1999b) anywhere in the C skeleton probably does not create as much strain as the conversion of an sp^2 to sp^3 site. Therefore, it is reasonable to expect that an O atom can attach anywhere on a typical PAH^+ skeleton, whether or not there is already an H atom attached to the carbon. It is worth noting as support for this picture that the fullerene C_{60}^+ cation has been reported to react with O to form an epoxide association product (Creegan et al. 1992).

All experiments carried out on PAH cations were done using PAH^+ in a state of hydrogenation close to the optimal value expected for a normal PAH (one H atom on each peripheral carbon atom that is not attached to an internal carbon). The doubly dehydrogenated naphthalene and pyrene cations were found to have almost the same reactivity as the corresponding PAH cations, and thus it is assumed that dehydrogenated radical PAH cations have the same reactivities as normal PAH cations. This is extended to any PAH^+ missing an even number of hydrogen atoms. For reactions between singly dehydrogenated PAH^+ and H_2, a rate coefficient at 300 K of 5×10^{-11} cm^3 s^{-1} is assumed, based on the experimentally measured reactivities of the phenylium and naphthylium cations.

This approach is also extended to more extensively dehydrogenated PAH^+ species with an odd number of missing hydrogen atoms. For reactions between these species and atomic hydrogen, a rate coefficient of 5×10^{-11} cm^3 s^{-1} was chosen based on experimental results for the naphthalene system.

Small highly hydrogenated PAH cations are not reactive with molecular hydrogen, and it is assumed that this behavior holds for larger PAH^+ as well. By contrast, these species do react slowly with atomic hydrogen, at a rate of $\sim 10^{-12}$ cm^3 s^{-1} (Snow et al. 1998). It was found experimentally that these hydrogenated PAH^+ species can be further hydrogenated at this same small rate, and these processes have been included in the model.

Finally, it should be noted that recent experimental measurements of the reactivity of small hydrocarbon cations toward H or H_2 (Scott et al. 1997) showed that usually these species react either with H or H_2 and thus it was concluded that in environments where significant amounts of both atomic and molecular hydrogen coexist, production of highly saturated hydrocarbons is expected. Furthermore, the well-known lack of reactivity of small hydrocarbon cations with H_2 in many cases (Giles et al. 1989) was interpreted as due to insufficient degrees of freedom for the cations to efficiently stabilize the association product. This should not be the case for large PAH cations, however, which have many degrees of freedom available (Scott et al. 1997). Figure 14 summarizes the reactivity of small PAH cations with atoms.

3.5. *Minor Processes*

In our model we take into account only those processes which are fast enough to compete with the typical hydrogenation rate of PAH cations (i.e., processes which alter the molecule on timescales shorter than a few hundred years). We can distinguish four additional processes which occur in diffuse clouds, but with such slow rates that the hydrogenation steady state distribution dictated by the four major processes discussed above is not affected. These four minor processes are electron attachment, which produces PAH anions; photodissociation with ejection of carbon-containing molecules; production of PAH^{++} when the second ionization potential is lower than 13.6 eV; and chemistry between PAH^+ and O and N atoms or between PAH and C^+.

3.5.1. *Electron Attachment and Photodetachment*

To evaluate the proportion of anions in the PAH distribution we compare the different rates which produce and destroy the anions with respect to neutrals. Two important rates are k_e, the rate at which electrons attach to neutral PAHs to form PAH^-, and k_p, the photodetachment rate due to absorption of a VIS/UV photon. Omont (1986) has estimated the electron attachment rate to be

$$k_e = Y_a 2\pi \left(\frac{\alpha e^2}{m_e}\right)^{1/2}, \tag{20}$$

where Y_a is the sticking coefficient of the electron onto the PAH, α is the polarizability of the PAH, and e and m_e are the charge and mass of the electron, respectively. Assuming

a sticking coefficient of 1 for large molecules and a polarizability $\alpha = 0.9\ (N_c)^{3/2}\ A^3$ from the π electrons yields the numerical estimate

$$k_e = 10^{-7}(N_C)^{3/4}\ \mathrm{cm}^3\ \mathrm{s}^{-1}\ , \tag{21}$$

where N_C is the number of carbon atoms.

There is another estimate of k_e derived from a different formula for PAH polarizability (Allamandola et al. 1989), but the predictions are within a factor 2 for PAHs with $N_C < 100$. Thus, this approach will not be considered here.

The electron photodetachment rate is more difficult to estimate due to the lack of experimental data on the cross sections. However, the cross section for atomic ions typically lies in the range 10^{-18}–10^{-16} cm^2 (Pegg 1996), and we can make a very conservative estimate using the same value as the ionization cross section for neutrals, i.e., $\sigma_{\mathrm{ion}} \sim 2 \times 10^{-18}$ cm^2 per C atom. A rough estimate of the photodetachment rate in the ISM is given by the expression

$$k_p = \sigma_{\mathrm{ion}} N_C N_{\mathrm{ph}}\ , \tag{22}$$

where N_{ph} is the total number of photons in the Draine field model between the threshold for photodetachment (i.e., the electron affinity of the neutral) and 13.6 eV. For an electron affinity of about 3 eV, N_{ph} is about 10^9 photons eV^{-1} cm^{-2} s^{-1}, and thus the ratio r_n of anions to neutrals for a PAH is

$$r_n = \frac{k_e n_e}{k_p}\ . \tag{23}$$

For a typical H atom density of 25 cm^{-3} and for a PAH bearing 25 carbon atoms, this ratio has the value 7.8×10^{-2}. Thus, while not negligible, the compact PAH anions are usually in lower concentration than the neutrals. However, the anions will be much more important, possibly dominant, in dense clouds (Lepp & Dalgarno 1988).

The anion fraction in diffuse clouds may be even lower, because in the calculation above for electron attachment, the sticking coefficient is chosen to be equal to unity, an assumption which is probably valid only for large PAHs (Dartois & d'Hendecourt 1997; Allamandola et al. 1989).

It should be emphasized that the calculations above apply only to compact (pericondensed) PAHs. For catacondensed PAHs such as pentacene, the anion population could be higher, and possibly be the major charge state (Salama et al. 1996). However, catacondensed PAHs are thought to be less stable in the ISM, and might be converted to the more stable compact PAHs (Wang et al. 1997; Dartois & d'Hendecourt 1997). Therefore, we conclude that PAH neutrals outnumber PAH anions, and that the anion proportion can be deduced directly from the corresponding neutral proportion without considering any "coupling effect" which may arise from the anion chemistry.

However, we should also compare the anion density to the cation density, because the anions might also be reactive with H and H_2. The ratio $r_{-/+}$ of anions to cations is given by

$$r_{-/+} = \frac{k_e n_e k_{\mathrm{rec}} n_e}{k_p k_{\mathrm{ion}}}\ , \tag{24}$$

where k_{rec} is the recombination rate between PAH^+ and electrons, and k_{ion} is the ionization rate of neutral PAHs. For the recombination rate of PAH^+ we have taken the experimental value of Abouelaziz et al. (1993) of 10^{-6} cm^3 s^{-1} for $C_6H_6^+$. For k_{ion} we estimate the ionization cross section to be about 2×10^{-18} cm^2 per C atom. We estimate the number of photons from the Draine field that have an energy higher than 7 eV to be $\sim 10^8$ photons eV^{-1} cm^{-2} s^{-1}. Thus, for a PAH bearing N_c carbons the ratio is given by

$$r_{-/+} = 8.5 \times 10^{-3} n_{\mathrm{H}}^2 N_C^{-5/4}\ . \tag{25}$$

For a 25-carbon PAH with $H = 25$ cm^{-3}, this expression gives $r_{-/+} = 9.5 \times 10^{-2}$.

Therefore, PAH anions appear to be much less common than either neutrals or cations in normal diffuse clouds, and thus we do not include any processes in our model which involve anions. We do not claim that anions are totally absent from the diffuse interstellar medium. However, we do claim that PAH anion densities are usually too low to alter the hydrogenation state of the PAH distribution, because the PAHs exist preferentially as cations which react readily with atomic hydrogen.

As a passing comment related to this, if C_7^- is present in the interstellar medium as has been suggested (Kirkwood et al. 1998), we expect C_7^+ to be present at an even higher level. Moreover, C_7 is known to have a high electron affinity (3.3 eV). For common PAHs such as naphthalene, anthracene, or pyrene, the low EA (less than 1 eV) makes the anionic form of these PAHs even less important than for C_7, due to the greater number of photons which have sufficient energy to photodetach weakly bound electrons. Hence, it is likely that the chemistry of PAHs in the diffuse ISM is dominated by cations rather than anions.

3.5.2. *Photodissociation with Carbon Loss*

Of all approximations discussed here, the neglect of the carbon loss channel after UV absorption appears to be the most questionable. In their two-laser experiment for the study of unimolecular decay of the benzene cation, Kühlewind et al. (1986) found a dissociation channel with C_2H_2 loss in the 5 eV range of internal energy, which is of the same order of magnitude as the hydrogen loss channel. This channel was expected to be the major dissociation channel at higher energies. In the experiments of Lifshitz and coworkers on naphthalene (Ho et al. 1995) and on anthracene and phenanthrene (Ling & Lifshitz 1998), the C_2H_2 loss channel also appeared to be of the same order of magnitude as the H loss channel.

However, in their study of the pyrene cation, Ling et al. (1995) noted that acetylene loss was too small to be accurately measured and they reported only the H and H_2 loss channels. Similarly, Jochims (1994) was not able to detect the C_2H_2 loss channel for the compact coronene cation, even though the H loss channel was effectively seen and characterized (Allain et al. 1996a, 1996b).

Despite these findings, it is possible that the C_2H_2 loss channel is significant, primarily for catacondensed PAH^+ species where the PAH^+ ends are more exposed than in the more compact (pericondensed) PAHs such as pyrene. This is consistent with the idea that compact PAHs are more important in the ISM due to their greater resistance to dissociation (Wang et al. 1997). UV photons may thus convert catacondensed PAH or branched PAH species into the more compact pericondensed PAH. In view of this argument, it appears that the neglect of C_2H_2 loss is a reason-

able hypothesis which should not strongly affect the results of our model.

3.5.3. *Reactions with* O, N, *and* C^+

The typical lifetime of a PAH^+ with respect to the O atom addition reaction is

$$\tau_O = \frac{1}{k_O[O]}, \tag{26}$$

where k_O is the rate of addition of O atoms to PAH^+ and [O] is the density of O atoms in diffuse clouds. For a hydrogen density of 25 cm^{-3} and an O/H ratio of 3.0×10^{-4}, the lifetime is about 4×10^4 yr and not likely to affect the hydrogenation rate. However, as in the case of C_2H_2 loss, this process may have an effect only after the hydrogenation steady state distribution has been reached.

Reactions with N atoms are even less likely to occur, due to the spin conservation law, and will be effective only for PAH distributions where a triplet state is present at a sufficiently high level, as in the case of dehydrogenated pyrene cation, for example (Le Page et al. 1999a).

Reactions between C^+, the only carbon species to be considered if we assume that all carbon atoms are locked into the cationic form, and PAHs have been studied in the case of anthracene by Canosa et al. (1995), who reported a reaction rate coefficient equal to the Langevin rate of 3×10^{-9} cm^3 s^{-1}. Hence, the lifetime of such a PAH with respect to reaction with C^+ is $\tau_{C^+} \sim 3 \times 10^3$ yr, which is far longer than the hydrogenation migration time in most cases.

3.5.4. *Double Ionization of PAH*

Leach (1987) has pointed out that PAH^{++} forms are also relevant to the interstellar medium, due to the typically low (<13.6 eV) ionization potential of singly charged PAH cations. However, the energy needed to form a doubly charged PAH from a singly charged PAH is generally close to 13.6 eV, and there are few photons in this narrow energy range which can produce such species. In the case of coronene (one of the PAHs with the smallest difference in energy between the first and second ionization potential in the study of Tobita and coworkers), a photon of 11.5 eV is required to produce the doubly charged cation. There are only a few million photons (in units of cm^{-2} s^{-1}) with an energy above this threshold in the interstellar UV field measured by Draine (1978). If we assume an ionization cross section of about 10^{-16} cm^2 for coronene then the lifetime of the PAH^+ will be more than about a hundred years and thus this process will probably not affect the hydrogenation distribution rate.

4. DESCRIPTION OF THE MODEL

We have developed a simple model in order to find the hydrogenation state of any PAH in the ISM, depending on the environmental parameters. This model assumes a steady state distribution for the PAH densities ($t \rightarrow \infty$). This assumption has been checked using another time-dependent model based upon Markov chains.

4.1. *The Steady State Model*

In our model we neglect processes which destroy the carbon skeleton of the PAH^+ under investigation, and thus the total number of the PAH^+ hydrogen derivatives is constant. The density of each PAH is determined by the kinetic equation

$$\frac{d[PAH_n^{(+)}]}{dt} = -\sum \text{loss processes} + \sum \text{growth processes} . \tag{27}$$

We have a set of $2y + 1$ equations, one for each hydrogenation state which is in the range 0 to $2y$ if y is the normal hydrogen coverage of the PAH (e.g., $y = 12$ for coronene), and for each charge state of the PAH (cation and neutral) we have two equations, thus leading to a matrix of $4y + 2$ equations. All these equations can be placed together on a single kinetic matrix $[K]$ whose generic coefficient $K(i, j)$ represents the contribution of the PAHs in hydrogenation and charge state j to the PAH in state i through all type of reactions (with the new convention that even indices are for cations and odd indices are for neutrals rather than using superscripts for the charge state). These equations are coupled because every process affecting a given PAH completely redistributes the amount of this PAH that is lost by reaction among the other hydrogenation and charge states. We thus replace one of the coupled equations above with an equation of mass conservation

$$\sum_{i=1}^{4y+2} [PAH_i] = 1 . \tag{28}$$

In the kinetic matrix all $K(i, j)$ will depend on the specific environment (n_H, n_{H_2}, T, UV field, n_e). The steady state distribution $[X]$ of hydrogenation states for a specific PAH is a solution of the equation

$$[K'][X] = [B] , \tag{29}$$

where $[K']$ is the kinetic matrix $[K]$ with one equation substituted with equation (28), $[B]$ is a vector with all the $4y + 2$ coefficients set equal to 0 (for the steady state distribution, every density is constant and thus each $d[PAH_i]/dt$ is equal to 0), except for the last coefficient which is set to 1 in agreement with the mass conservation equation.

The matrices are generated and the model is solved using the Scilab-2.3[2] program package from INRIA (the French National Institute of Research in Computer Engineering) and the steady state distribution is given for any chosen environment.

4.2. *Time Dependence*

In order to test the validity of the steady state model described above, the time needed for any PAH to reach its steady state distribution is evaluated. This serves as a check that the steady state distribution of hydrogenation states will be reached in a time shorter than the characteristic time required for any other perturbing process.

To do this, we present here another model, which calculates the time-dependent chemistry of PAHs in the ISM. Such an alternative model is expected to converge to the

[2] Scilab 2.3. 1997, INRIA-rocquencourt. Available at http://www-rocq.inria.fr/scilab/.

time-independent steady state model. The steady state model is justified if the time for which the convergence is attained is shorter than typical times for perturbing processes which were calculated at the end of § 3. The validity of the steady state model is illustrated in the Appendix using $C_{50}H_n$ as a simple example.

Processes affecting the PAH distribution in the ISM can be viewed as Markov processes (see, e.g., Norris 1997), because only the current state of the distribution can affect its future (i.e., the system retains no memory of the past). We thus examine how the system evolves in a typical time τ that is small with respect to all characteristic times of physical processes in the ISM.

The stochastic matrix $[S]$ whose coefficients are calculated for this typical time τ transforms a PAH distribution characterized by the vector $[X]$ onto the next one after the elapsed time τ:

$$[X_{n+1}] = [S][X_n] . \tag{30}$$

This stochastic matrix is related to the K matrix according to the equation

$$[S] = [I] + \tau(t([K])) , \tag{31}$$

where $[K]$ is the kinetic matrix formed of all coupled equations (i.e., eqs. [27] and [28]). The matrix $t([K])$ is the transposed matrix of $[K]$ and $[I]$ is the identity matrix.

When n is very large the distribution will tend to the steady state distribution:

$$[X_{n\to\infty}] = [S]^n[X_0] = [K']^{-1}[B] . \tag{32}$$

To estimate the value of n for which this steady state distribution is reached, we choose to compare the distribution calculated using the stochastic matrix and the steady state distribution.

It is assumed that the steady state distribution is approximately reached for a given n when the sum of the absolute differences between the coefficient of the Markov distribution $[X_n]$ and the steady state distribution is less than 0.3, while starting from a uniform distribution for the initial Markov distribution with every coefficient set to $1/(4y + 2)$ (a somewhat lower value than 0.3 will not drastically affect the computation). A simple example which shows how the two models are related is given in the Appendix.

5. CONCLUSION

In this paper we have presented a new model of PAH chemistry in diffuse clouds which takes advantage of recent experiments on PAH photodissociation as well as PAH cation chemistry. The model takes into account the major processes that PAHs undergo in diffuse cloud environments, such as ionization, electron recombination, photodissociation, and chemistry involving the H and H_2 species. A simple approach to photodissociation based on the RRKM theory has been presented and tested using recent experiments carried out on PAH cations. This procedure has been proposed as a simple tool for an evaluation of the branching ratio of PAH^+ dissociative recombination with electrons. Finally, after a description of a simple time-independent steady state model, a more elaborate time-dependent model based upon Markov's chain has been presented.

In Paper II we report the results of model calculations for realistic diffuse ISM conditions, and discuss their relevance to the diffuse band problem, the UIRs, and general ISM chemistry and physics.

We are grateful to Emma Bakes for her careful reading of an earlier version of this manuscript which led to many improvements. This research was sponsored by the National Aeronautics and Space Administration. Computational support was provided by the National Science Foundation (CHE-9734867).

APPENDIX

We present here a simple example of how the model works and how the two models based upon Markov chains and upon the steady state model are related. For purposes of illustration we choose the $C_{50}H_n$ generic PAH. This species can exist in many different hydrogenation states but the density is concentrated in only the three major states which are $C_{50}H_{20}$ (the PAH with normal hydrogen coverage), $C_{50}H_{20}^+$ and $C_{50}H_{21}^+$. The major processes affecting these PAHs are represented in Figure 15. The steady state distribution can be calculated using only these three major species. If we assume a hydrogen density of 50 cm^{-3} and a n_e/n_H ratio of 1.4×10^{-4} (with $n_H = [H] + 2[H_2] = 100\ cm^{-3}$) the above rates k_{ion}, $k_{rec}n_e$, $k_{diss,H}$ and $k_{add,H}[H]$ will have the values 0.052, 0.019, 0.022, and 0.011 in the units of $month^{-1}$. The generic coefficient $K_{i\neq j}$ of the kinetic matrix $[K]$ represents the proportion of PAH_j which is converted into PAH_i after the elapsed time of one month, while the generic negative coefficient K_{ii} represents the overall loss of PAH_i during one month, taking into account all processes. We also replace the last row of the kinetic matrix with the mass conservation equation (eq. [28]) stating that the total density of PAH is constant. In order to find the steady state distribution we solve the following equation:

$$\begin{bmatrix} -k_{rec}\,n_e - k_{add,H}[H] & k_{ion} & k_{diss,H} \\ k_{rec}\,n_e & -k_{ion} & k_{rec}\,n_e \\ 1 & 1 & 1 \end{bmatrix} \times \begin{bmatrix} C_{50}\,H_{20}^+ \\ C_{50}\,H_{20} \\ C_{50}\,H_{21}^+ \end{bmatrix} = \begin{bmatrix} 0 \\ 0 \\ 1 \end{bmatrix}$$

where $[C_{50}H_n^{(+)}]$ represents the relative density of the PAH $C_{50}H_n^{(+)}$ when the steady state distribution is reached. For an H density of 50 cm^{-3} and for a n_e/n_H ratio of 1.4×10^{-4} the above equation can be solved and the steady state distribution corresponds to 57% $C_{50}H_{20}^+$, 27% $C_{50}H_{20}$, and 16% $C_{50}H_{21}$. This is in very good agreement with the results from the full computation presented in Paper II.

The alternative time-dependent model is based on the stochastic matrix which is related to the kinetic matrix above through equation (31). In this matrix the generic coefficient S_{ii} represents the proportion of PAH_i that is not affected after one

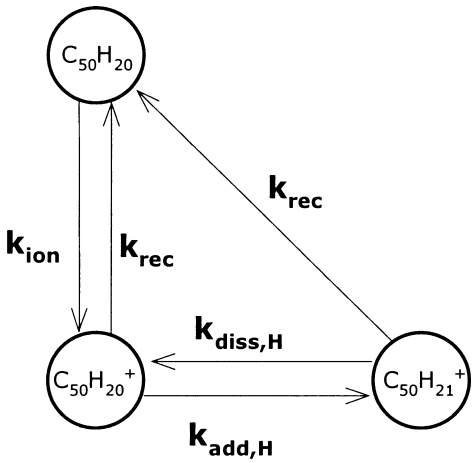

FIG. 15.—Processes affecting a large PAH distributed in three major hydrogenation and charge states. k_{ion} and k_{rec} are the rate of ionization of the neutral and the rate of recombination of the cations with electrons, while $k_{diss,H}$ and $k_{add,H}$ are the rates of photodissociation and H addition, respectively.

month while the generic $S_{i\neq j}$ coefficient represents the contribution of PAH_i to PAH_j (we thus have $S_{i\neq j} = K_{j\neq i}$). Therefore, this stochastic matrix has the following form in the case of our simplified model of $C_{50}H_n$:

$$S_0 = \begin{bmatrix} 1 - (k_{rec}\, n_e + k_{add,H}[H]) & k_{rec}\, n_e & k_{add,H}[H] \\ k_{ion} & 1 - k_{ion} & 0 \\ k_{diss,H} & k_{rec}\, n_e & 1 - k_{diss,H} - k_{rec}\, n_e \end{bmatrix}.$$

Given the relative initial proportion of $C_{50}H_{20}^+$, $C_{50}H_{20}$, and $C_{50}H_{21}^+$, this stochastic matrix expresses the way that any specific distribution is affected after a period of one month. The square of this matrix gives the distribution after 2 months while the nth power of this matrix gives the distribution after 2^n months. For the model to work properly it is important that the S_{ii} coefficients in the S_0 matrix are close to 1 due to the convergence constraint. With the above numerical values the distribution will be close to the steady state distribution for $n = 5$:

$$S_5 = \begin{bmatrix} 0.576 & 0.265 & 0.158 \\ 0.581 & 0.273 & 0.144 \\ 0.546 & 0.265 & 0.188 \end{bmatrix}.$$

If we allow more time, the distribution approaches the steady state distribution which is reached when every row contains the same numbers. For example, for $n = 8$ each number in a given column of the matrix will be equal up to the fourth decimal place, with the same values as those calculated in the case of the steady state distribution (approximately 57%, 27%, and 16% for $[C_{50}H_{20}^+]$, $[C_{50}H_{20}]$, and $[C_{50}H_{21}^+]$, respectively). Thus, for the specific case described here the migration time can be roughly approximated as the time corresponding to the S_5 matrix, that is about $2^{(5+1)} = 64$ months ~ 5 yr. For a complete calculation with the model taking into account all hydrogenation states this migration time is somewhat larger due to the time needed for the dehydrogenated species to form the $C_{50}H_{20,21}^{(+)}$ species through consecutive H addition.

REFERENCES

Abouelaziz, H., Gomet, J. C., Pasquerault, D., Rowe, B. R., & Mitchell, J. B. A. 1993, J. Chem. Phys., 99, 237
Adams, N. G. 1994, Int. J. Mass Spectrom. Ion Processes, 132, 1
Allain, T., Leach, S., & Sedlmayr, E. 1996a, A&A, 305, 602
———. 1996b, A&A, 305, 616
Allain, T., Sedlmayr, E., & Leach, S. 1997, A&A, 323, 163
Allamandola, L. J., Tielens, A. G. G. M., & Barker, J. R. 1989, ApJS, 71, 733
Ausloos, P., Lias, S. G., Buckley, T. J., & Rogers, E. 1989, Int. J. Mass Spectrom. Ion Processes, 92, 65
Bahcall, J. N., & Woolf, R. A. 1968, ApJ, 152, 701
Bakes, E. L. O., & Tielens, A. G. G. M. 1994, ApJ, 427, 822
Barker, J. R. 1980, J. Chem. Phys., 72, 3686
Bates, D. R. 1988, in Molecular Astrophysics, ed. T. W. Hartquist (Cambridge: Cambridge Univ. Press), 211
Bettens, R. P. A., & Herbst, E. 1995, Int. J. Mass Spectrom. Ion Process., 149, 321
———. 1996, ApJ, 468, 686
Buch, V. 1989, ApJ, 343, 208
Canosa, A., Laubé, S., Rebrion, C., Pasquerault, D., Gomet, J. C., & Rowe, B. R. 1995, Chem. Phys. Lett., 245, 407
Capron, L., Mestdagh, H., Rolando, C., & Sablier, M. 1994, 42d ASMS Conference on Mass Spectrometry & Allied Topics, p. 550
Cherchneff, I., Barker, J. R., & Tielens, A. G. G. M. 1991, ApJ, 377, 541
———. 1992, ApJ, 401, 269
Crawford, M. K., Tielens, A. G. G. M., & Allamandola, L. J. 1985, ApJ, 293, L45
Creegan, K. M., et al. 1992, J. Am. Chem. Soc., 114, 1103
Dartois, E., & d'Hendecourt, L. 1997, A&A, 323, 534
Draine, B. T. 1978, ApJ, 36, 595
Draine, B. T., & Sutin, B. 1987, ApJ, 320, 803
Duley, W. W., & Williams, D. A. 1984, Interstellar Chemistry (New York: Academic Press)
Dunbar, R. C. 1990, Int. J. Mass Spectrom. Ion Processes, 100, 423
———. 1997, Int. J. Mass Spectrom. Ion Processes, 169, 1
Feng, W. Y., & Lifshitz, C. 1996, Int. J. Mass Spectrom. Ion Processes, 152, 157
Fleming, I. 1976, Frontier Orbitals and Organic Chemical Reactions (New York: Wiley)
Forst, W. 1973, Theory of Unimolecular Reactions (New York: Academic)
Frenklach, M., & Feigelson, E. D. 1989, ApJ, 341, 372
———. 1997, in ASP Conf. Ser. 122, From Stardust to Planetesimals, ed. Y. Pendleton & A. G. G. M. Tielens (San Francisco: ASP), 107
Frisch, M. J., et al. 1995, Gaussian 94 (Revision C.2; Pittsburgh: Gaussian, Inc.)
Galazutdinov, G. A., Krelowski, J., & Musaev, F. A. 1999, MNRAS, 310, 1017
Giles, K., Adams, N. G., & Smith, D. 1989, Int. J. Mass Spectrom. Ion Processes, 89, 303
Gotkis, Y., Naor, M., Laskin, J., Faulk, J. D., & Dunbar, R. C. 1993a, J. Am. Chem. Soc., 115, 7402
Gotkis, Y., Oleinikova, M., Naor, M., & Lifshitz, C. 1993b, J. Phys. Chem., 97, 12282
Habing, H. J. 1968, Bull. Astron. Inst. Netherlands, 19, 421

Harvey, J. N., Aschi, M., Schwarz, H., & Koch, W. 1998, Theor. Chem. Acc., 99, 95
Heger, M. L. 1922, Lick Obs. Bull., 377, 146
Herbst, E., & Dunbar, R. C. 1991, MNRAS, 253, 341
Herbst, E., & Le Page, V. 1999, A&A, 344, 310
Ho, Y.-P., Dunbar, R. C., & Lifshitz, C. 1995, J. Am. Chem. Soc., 117, 6504
Holbrook, K. A., Pilling M. J., & Robertson, S. H. 1996, Unimolecular Reactions (2d ed.; New York: Wiley)
Hrusák, J., Schröder, D., & Iwata, S. 1997, J. Chem. Phys., 106, 7541
Illenberger, E., & Momigny, J. 1992, Topics in Physical Chemistry Vol. 2 (New York: Springer)
Jeffreys, H., & Jeffreys, B. S. 1956, Methods of Mathematical Physics (Cambridge: Cambridge Univ. Press)
Jenkins, E. B., & Shaya, E. J. 1979, ApJ, 231, 55
Jenniskens, P., & Désert, F.-X. 1993, A&AS, 106, 39
———. 1994, A&A, 274, 465
Joblin, C. 1992, Ph.D. thesis, Univ. Paris
Jochims, H. W., Rühl, E., Baumgärtel, H., Tobita, S., & Leach, S. 1994, ApJ, 420, 307
Kiefer, J. H., Mizerka, L. J., Patel, M. R., & Wei, H. -C. 1985, J. Phys. Chem., 89, 2013
Kirkwood, D. A., et al. 1998, Faraday Discuss., 109 (London: Royal So. Chem.), 109
Klippenstein, S. J. 1997, Int. J. Mass Spectrom. Ion Processes, 167, 235
Klippenstein, S. J., Faulk, J. D., & Dunbar, R. C. 1993, J. Chem. Phys., 98, 243
Kühlewind, H., Kiermeir, A., & Neusser, H. J. 1986, J. Chem. Phys., 85, 4427
Kühlewind, H., Kiermeir, A., Neusser, H. J., & Schlag, E. W. 1987, J. Chem. Phys., 87, 6488
Leach, S. 1987, in Polycyclic Aromatic Hydrocarbons and Astrophysics, ed. A. Léger, L. d'Hendecourt, & N. Boccara (Dordrecht: Reidel), 99
Léger, A., Boissel, P., Désert, F. X., & d'Hendecourt, L. 1989, A&A, 213, 351
Léger, A., & d'Hendecourt, L. 1985, A&A, 146, 81
Léger, A., & Puget, J. L. 1984, A&A, 137, L5
Le Page, V., Keheyan, Y., Bierbaum, V. M., & Snow, T. P. 1997, J. Am. Chem. Soc., 119, 8373
Le Page, V., Keheyan, Y., Snow, T. P., & Bierbaum, V. M. 1999a, Int. J. Mass Spectrom., 185, 949
Le Page, V., Keheyan, Y., Snow, T. P., & Bierbaum, V. M. 1999b, J. Am. Chem. Soc., 121, 9435
Le Page, V., Snow, T. P., & Bierbaum, V. M. 2001, in preparation (Paper II)
Lepp, S., & Dalgarno, A. 1988, ApJ, 324, 553
Lias, S. G., Bartmess, J. E., Liebman, J. F., Holmes, J. L., Levin, R. D., & Mallard, W. G. 1988, J. Phys. Chem. Ref. Data, 17, suppl. 1
Lifshitz, C. 1987, Adv. Mass Spectrom., 9, 1
———. 1989, Adv. Mass Spectrom., 11, 713
Ling, Y., Gotkis, Y., & Lifshitz, C. 1995, Eur. Mass Spectrom., 1, 41
Ling, Y., & Lifshitz, C. 1998, J. Phys. Chem. A, 102, 708
Ling, Y., Martin, M. L., & Lifshitz, C. 1997, Int. J. Mass Spectrom. Ion Processes, 160, 39
Mathis, J. S. 1997, in ASP Conf. Ser. 122, From Stardust to Planetesimals, ed. Y. Pendleton & A. G. G. M. Tielens (San Francisco: ASP), 87
Mathis, J. S., Mezger P. G., & Panagia, N. 1983, A&A, 128, 212
McCall, B. J., York, D. G., & Oka, T. 2000, ApJ, 531, 329
Mebel, A. M., Lin, M. C., Yu, T., & Morokuma, K. 1997, J. Phys. Chem. A, 101, 3196
Meyer, D. M., Cardelli, J. A., & Sofia, U. J. 1997, ApJ, 490, 103
Morton, D. C. 1975, ApJ, 197, 85
Motylewski, T., et al. 2000, ApJ, 531, 312
Nicolaides, A., Smith, D. M., Jensen, F., & L. Radom, L. 1997, J. Am. Chem. Soc., 119, 8083
Norris, J. R. 1997, Markov Chains (Cambridge: Cambridge Univ. Press)
Nourse, B. D., Cox, K. A., & Cooks, R. G. 1992, Org. Mass Spectrom., 27, 453
Omont, A. 1986, A&A, 164, 159
Pauzat, F., Talbi, D., Miller, M. D., DeFrees, D. J., & Ellinger, Y. 1992, J. Phys. Chem., 96, 7882
Pegg, D. J. 1996, in Atomic, Molecular, and Optical Physics Handbook, ed. F. G. W. Drake (New York: AIP), 681
Petrie, S., Javahery, G., & Bohme, D. K. 1992, J. Am. Chem. Soc., 114, 9205
Pino, T., Boudin, N., & Bréchignac, P. 1999, J. Chem. Phys., 111, 7337
Romanini, D., Biennier, L., & Stoeckel, F. 1999, Chem. Phys. Lett., 303, 165
Rowe, B. R., & Rebrion-Rowe, C. 1995, in Dissociative Recombination: Theory, Experiment and Applications III, ed. D. Zaifman, J. B. A. Mitchell, D. Schwalm, & B. R. Rowe (Singapore: World Scientific), 184
Rühl, E., Price, S. D., & Leach, S. 1989, J. Phys. Chem., 93, 6312
Salama, F., & Allamandola, L. J. 1992a, Nature, 358, 42
———. 1992b, ApJ, 395, 301
Salama, F., Bakes, E. L. O., Allamandola, L. J., & Tielens, A. G. G. M. 1996, ApJ, 458, 621
Sarre, P. J., Miles, J. R., Kerr, T. H., Hibbins, R. E., Fossey, S. J., & Sommerville, W. B. 1995, MNRAS, 277, L41
Scott, G. B. I., Fairley, D. A., Freeman, C. G., McEwan, M. J., Adams, N. G., & Babcock, L. M. 1997, J. Phys. Chem. A, 101, 4973
Sczcepanski, J., & Vala, M. 1993, ApJ, 414, 646
Snow, T. P., Le Page, V., Keheyan, Y., & Bierbaum, V. M. 1998, Nature, 391, 259
Sofia, U. J. 1997, in ASP Conf. Ser. 122, From Stardust to Planetesimals, ed. Y. Pendleton & A. G. G. M. Tielens (San Francisco: ASP), 77
Tielens, A. G. G. M., & Snow, T. P., eds. 1995, The Diffuse Interstellar Bands (Dordrecht: Kluwer)
van der Zwet, G., & Allamandola, L. J. 1985, A&A, 146, 76
Verstraete, L., Léger, A., d'Hendecourt, L., Dutuit, O., & Défourneau, D. 1990, A&A, 237, 436
Wang, X., Becker, H., Hopkinson, A. C., March, R. E., Scott, L. T., & Böhme, D. K. 1997, Int. J. Mass Spectrom. Ion Processes, 161, 69
Weston, R. E. 1986, Int. J. Chem. Kin., 18, 1259
York, D. G., & Kinahan, B. F. 1979, ApJ, 228, 127